https://doi.org/10.1070/RCR4896

Binary mixtures of semicrystalline polymers with low-molecular-mass compounds: thermal behaviour and phase structure

Konstantin V. Pochivalov,[a]* Andrey V. Basko,[a] Yaroslav V. Kudryavtsev [b]

[a] *G.A.Krestov Institute of Solution Chemistry, Russian Academy of Sciences, Akademicheskaya ul. 1, 153045 Ivanovo, Russian Federation*
[b] *A.V.Topchiev Institute of Petrochemical Synthesis, Russian Academy of Sciences, Leninsky prosp. 29, 119991 Moscow, Russian Federation*

The results of phase equilibrium studies in mixtures of semicrystalline polymers with low-molecular-mass compounds are summarized and analyzed. A new classification of phase diagrams for such mixtures is proposed. Alternative points of view on the phase composition of semicrystalline polymers are presented. The phase structure evolution during the thermally induced phase separation of mixtures is monitored and the morphology of the forming capillary porous bodies as precursors of polymeric membranes is described. The general regularities concerning the influence of the nature of mixture components, polymer molecular mass, temperature scanning rate and other factors on the topology of phase diagrams are considered. Experimental methods used to construct the phase diagrams of mixtures and to study features of their phase structure are compared.
The bibliography includes 203 references.

Contents

1. Introduction 311
2. Traditional description of a phase equilibrium 312
3. New description of a phase equilibrium 321
4. Differential scanning calorimetry in studies of phase equilibrium 328
5. Phase structure of mixtures of semicrystalline polymers with low-molecular-mass compounds 331
6. Conclusion 335

1. Introduction

The success of solving problems of polymer materials science associated with fabrication of items *via* polymer solutions and mixtures is largely associated with the availability of data on the phase equilibria and phase structures in these systems at various temperatures and compositions.[1,2]

K.V.Pochivalov. Doctor of Chemical Sciences, Chief Researcher at the ISC RAS.
Telephone: +7(4932)35 – 1879, e-mail: pkv@isc-ras.ru
A.V.Basko. PhD Student, Intern Researcher at the ISC RAS.
Telephone: +7(4932)35 – 1879, e-mail: avb@isc-ras.ru
Current research interests of the authors: physical chemistry of polymers, phase equilibria in polymer – liquid systems, phase structure, morphology of polymeric membranes, phase diagrams, polymer materials science, structure – property relationships, modification of polymers.
Y.V.Kudryavtsev. Doctor of Physical and Mathematical Sciences, Head of a laboratory of the TIPS RAS.
Telephone: +7(495)647 – 5927 ext. 237, e-mail: yar@ips.ac.ru
Current research interests: macromolecular reactions, kinetics, copolymers, multicomponent systems, structure – property relationship, phase diagrams, theory and modelling.

Translation: Z.P.Svitanko

The fundamentals of the theory of phase equilibria in binary mixtures of low-molecular-mass liquids formulated by Gibbs[3] were later supplemented and extended by Schreinemakers[4] and van der Waals and Kohnstamm.[5] The authors of the last-mentioned book demonstrated for the first time that the liquid – liquid binodal in the phase diagram of mixtures of molecules of different masses is shifted towards compositions rich in the lower-molecular-mass component.

The principal concepts of thermodynamics of polymer solutions were developed in the early 1940s by Flory[6–8] and Huggins[9–11] in relation to the athermal mixing of a polymer with a low-molecular-mass liquid, which is not accompanied by a change in the system volume. Quite a number of later theoretical and experimental studies deal with upgrading the Flory – Huggins lattice model.[12–48] For example, Zimm *et al.*[14,15] derived the equation of state taking account of long-range interactions. Prigogine[16] and Patterson[17–19] proposed to include the change in the free volume upon component mixing. In the so-called Flory theory,[24–27] the configurational energy was determined by applying the Hirschfelder – Eyring approximation to a van der Waals liquid, with the distribution of solvent molecules and polymer chain segments being assumed to be uniform. The models that take into account the nonuniformity of this

Received 29 April 2019
© 2020 Uspekhi Khimii, ZIOC RAS, Russian Academy of Sciences and IOP Publishing Limited

mixing have been developed.[28–31] The applicability of the UNIFAC, UNIFAC-I, UNIFAC-II and UNIFAC-FV group models based on the assumption of additivity of contributions of various functional groups to the thermodynamic parameters of the system has been investigated.[20–23] These models consider the combinatorial contribution to the activity coefficient, the free volume and the temperature dependence of energy parameters in different ways.

Sanchez and Lacombe[34] proposed a lattice model that took into account the compressibility, specific interactions (such as hydrogen bonds) and the change in the molecular architecture to improve the agreement between the calculated and experimental data.

Qian *et al.*[35,36] proposed separating the Flory–Huggins interaction parameter into two contributions, which reflect its dependence on the composition and temperature. This allowed them to predict the existence of systems with liquid–liquid binodal curves with both upper and lower critical solution temperatures.

Chen[37] and Vetere[38] used a combination of the Flory–Huggins model with the two-liquid theory, which included the enthalpy contribution to the interaction between the components, Orbey and Sandler[39] combined it with a three-parameter cubic equation of state, which took account of the number of external degrees of freedom. Subsequently, the Flory–Huggins theory was advanced by calculation of the thermodynamic properties of mixtures containing associates and allowance for the attractive and repulsive interactions.[40,41]

Publications that appeared in the beginning of the 21st century[42,43] were based on the assumption of possible incorporation of solvent molecules into polymer crystallites, which required introducing a new parameter for the crystal–amorphous interaction. Malik *et al.*[44] experimentally showed that the interaction of a semicrystalline polymer with a low-molecular-mass component can give so-called clathrates, intercalates or crystal solvates. Anthamatten[45] introduced a new parameter into the Flory–Huggins theory to take into account the contribution of the terminal groups to the interaction of components.

The theoretical studies dealing with polymer solutions published before 1980 were summarized in a monograph[46] where one chapter is devoted to calculation of thermodynamic parameters derived from phase diagrams by various methods: from positions of binodal and spinodal curves, melting point depression and vapour sorption data, by reverse phase gas chromatography, *etc*. Later publications are analyzed in a review.[47]

It is noteworthy that because of insignificant difference between the predictive powers of the above-mentioned models, most researchers still use the simplest classical Flory–Huggins theory for quantitative description of phase diagrams;[1,48–50] however, like the modified versions, the pristine theory does not always adequately describe experimental data. In particular, there is still no universal equation for predicting the phase composition of an arbitrary system containing a polymer and a low-molecular-mass component (liquid or crystalline solid). Analysis of phase equilibrium is often performed using a phenomenological approach traditional for physical chemistry, which is based on a topological analysis of experimental phase diagrams[51–53] and provides qualitative data on the phase composition and physical state of these systems over a broad range of temperatures and concentrations.

Some publications summarize the data on phase equilibria and phase transitions in polymer blends[1] and polymer solutions located in a mechanical field.[54] Meanwhile, to our knowledge, analysis of phase equilibrium of this type in semicrystalline polymer mixtures with low-molecular-mass liquids or crystalline solids has not yet been reported in Russian or foreign sources. The present work is intended to fill this gap.

Now there are two concepts of phase equilibria in the indicated systems, which differ crucially in the interpretation of the physical state of semicrystalline polymers. Therefore, we consider it expedient to discuss both concepts and to leave the reader to decide which is more well-posed.

The following abbreviations are used in the review:
DBP — dibutyl phthalate,
DEP — diethyl phthalate,
DMTP — dimethyl terephthalate,
DNAP — 2,4-dinitro-2,4-diazapentane,
DOP — dioctyl phthalate,
DPE — diphenyl ether,
DSC — differential scanning calorimetry,
ECTFE — ethylene – chlorotrifluoroethylene copolymer,
EVOH — ethylene – vinyl alcohol copolymer,
HDPE — high-density polyethylene,
HMB — hexamethylbenzene,
iso-PP — isotactic polypropylene,
LCST —lower critical solution temperature,
LDPE — low-density polyethylene,
LMM — low-molecular-mass,
MM — molecular mass,
PBAMO — poly[3,3-bis(azidomethyl)oxetane],
PEG — polyethylene glycol,
PEO — poly(ethylene oxide),
PLA — polylactide,
PS — polystyrene,
PVDF — poly(vinylidene fluoride),
PVF — poly(vinyl fluoride),
SC — semicrystalline,
sPP — syndiotactic polypropylene,
TCB — 1,2,4,5-tetrachlorobenzene,
TIPS — thermally induced phase separation,
UCST — upper critical solution temperature,
UHMMPE — ultrahigh-molecular mass polyethylene,
T_m — melting temperature,
T_{cr} — crystallization temperature,
T_g — glass transition temperature,
w_2 — polymer mass fraction.

2. Traditional description of a phase equilibrium

The phase equilibrium in a linear polymer–liquid system was first described by Papkov, Kargin and Rogovin,[55] who studied the chloroform–cellulose diacetate couple. In experiments, they used one of the 14 fractions obtained from an industrial cellulose ester sample by a combination of fractional dissolution and precipitation methods. It was proved that the phase separation is reversible and that the gross composition of the coexisting phases does not depend on the way the equilibrium was achieved, that is, by heating or cooling of the component mixture. In other words, direct experimental evidence was obtained for applicability of the phase rule to solutions of amorphous polymers. The validity of this representation was confirmed almost simultaneously by studying mixtures of polystyrene (PS) and lauric acid esters.[56] Later, Papkov[52] extended this representation to

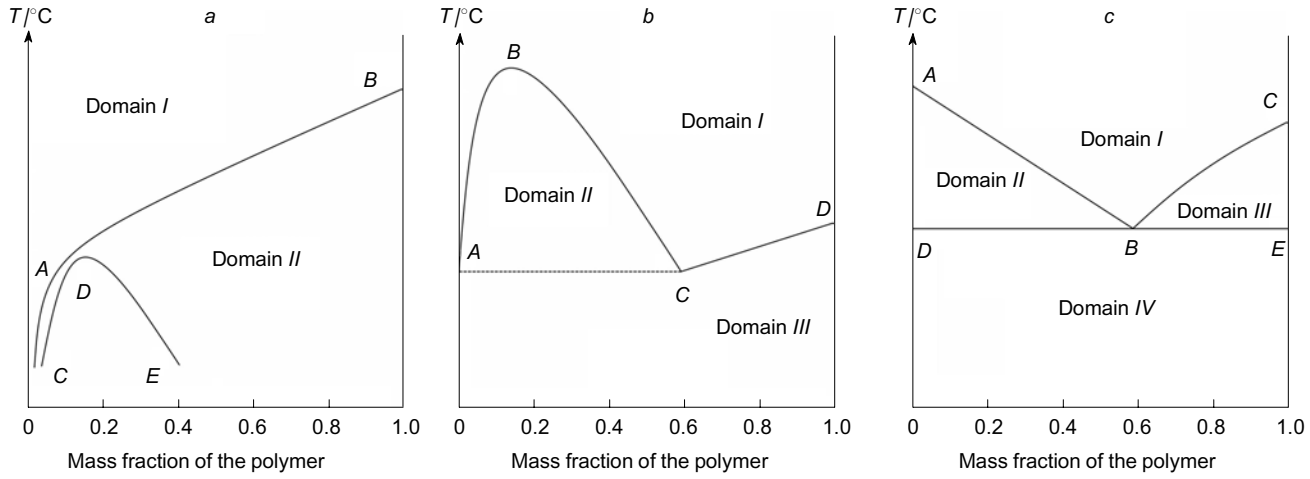


Figure 1. Schematic view of phase diagrams of SC polymer mixtures with good (*a*) and poor (*b*) solvents and with a crystalline LMM compound with the melting point close to the polymer melting temperature (*c*).
The diagrams were constructed within the context of the traditional interpretation of phase equilibria.[52]

semicrystalline (SC) polymer – liquid systems taking account of the results obtained by Richards[57] for mixtures of high-density polyethylene (HDPE) with xylene, nitrobenzene and amyl acetate. While discussing in detail the topology of phase diagrams of these systems, he presumed that these diagrams do not differ fundamentally from the diagrams of binary mixtures of low-molecular-mass (LMM) crystallizing liquids, but still have specific features related to the macromolecular nature of one of the components, in particular:

— the eutectic point is shifted along the axis of composition towards LMM liquid-rich mixtures, while along the axis of temperature, it virtually coincides with the melting point of this liquid;

— cooling of the system is accompanied by incomplete crystallization of the polymer, resulting in the separation of an imperfect crystalline phase, which includes both crystalline and amorphous regions;†

— the system has an increased tendency to supersaturation and supercooling due to low mobility of macromolecules, which hinders the formation of crystallites of the critical size acting as the nuclei;

— when the components are poorly compatible, a combination of the amorphous and crystalline coexistence regions may occur above the liquidus of the polymer.

Being based on the phase rule and taking into account the above-listed specific features and differences between crystallization rates of polymers, Papkov[52,58] classified the polymer – liquid systems in terms of their phase diagrams. We analyzed this classification with allowance for the fact that the phase diagram is a thermodynamic characteristic of a system that does not depend on the duration of relaxation processes. It turned out that mixtures of SC polymers with liquids may give rise to only two types of diagrams describing mixtures of SC polymers with good or poor solvents (Fig. 1 *a*,*b*).

† In Ref. 52, p. 67, it is noted that 'for principle consideration of the phase equilibrium, this imperfect crystallinity is of no significance, since this does not change the general behaviour of the equilibrium', that is, crystalline phase state is, in essence, postulated for SC polymers.

The diagram presented in Fig. 1 *a* characterizes the phase composition of a mixture of an SC polymer with a solvent; the amorphous phase separation domain bounded by binodal line *CDE* is located below liquidus *AB* of the polymer. It can be seen that the presumptive eutectic point is, in fact, markedly shifted towards LMM component-rich compositions. A single-phase system, that is, a polymer solution in the liquid, exists above line *AB* (domain *I*) and a two-phase system consisting of polymer crystallites and a polymer solution in the liquid occurs below this line (domain *II*). The state of the system below line *CDE* is beyond discussion. This domain obeys the lever rule, which can be used to determine the composition and mass fractions of the coexisting phases.

It was emphasized[52,58] that the amorphous phase separation domain can be detected only during cooling of the homogenized mixture, but not during heating of the initial system. In our opinion, this means that at least one of these lines is not equilibrium. Traditionally, it is believed that, if the binodal is measured experimentally, the system entering the domain below the binodal initially includes two phases that differ in the concentration of the polymer component in the solution and, after that, the polymer crystallizes in the polymer-rich phase to give defective crystallites.

The diagram presented in Fig. 1 *b* depicts the phase equilibrium in the SC polymer – solvent system in which the amorphous phase separation domain (domain *II*) bounded by binodal *ABC* is located above the liquidus line (*ACD*). In this case, the polymer and the solvent are poorly compatible even at temperatures above the minimum melting temperature of the mixture, which is characterized by monotectic point *C*. The domain above liquid – liquid binodal *ABC* with an upper critical solution temperature and liquidus line *CD* (domain *I*) corresponds to a single-phase solution of the polymer in the liquid. Two liquid phases coexist in the domain bounded by the binodal (domain *II*), while a solid (defective crystallites) and a liquid (polymer solution in the liquid) phase occur in the domain below line *CD* (domain *III*). The state of the system below line *AC* is beyond discussion.

Thus, in the context of Papkov's classification, the liquid – liquid binodal line with an upper critical solution

temperature (UCST) cannot be detected in the phase diagrams of SC polymer mixtures with a good solvent (Fig. 1 *a*), and it is shown in the picture below the polymer liquidus line from purely theoretical reasons.[59] In the phase diagrams of SC polymer mixtures with a poor solvent (see Fig. 1 *b*), the liquid – liquid coexistence line with an UCST is always located above the liquidus line. In the former case, only crystalline phase equilibrium exists in the system, while in the latter case, both amorphous and crystalline phase equilibria are present.

The types of phase diagrams described by Papkov should be supplemented by one more type, which reflects the phase composition of the mixtures in which the melting point of a crystalline LMM compound is close to the melting temperature of an SC polymer (Fig. 1 *c*). The phase diagrams of this type were first constructed by Smith and Pennings,[60] who studied the phase equilibrium of HDPE mixtures with hexamethylbenzene (HMB) and 1,2,4,5-tetrachlorobenzene (TCB). They contain liquidus lines for low- (curve *AB*) and high-molecular-mass (curve *BC*) components, a solidus line *DE* and eutectic point *B*. This point corresponds to coexistence of three phases (crystals of both components and their liquid mixture). According to the phase rule, the system at the eutectic point is invariant. Under the liquidus line on the LMM component-rich side (domain *II* in Fig. 1 *c*), crystals of this component coexist with a polymer solution in this component; under the liquidus line on the polymer-rich side (domain *III*), polymer crystallites coexist with the LMM solution; and under the solidus line *DE* (domain *IV*), the crystals of two components coexist.

The publications that we found for the period since 1946 (starting from the study of Richards [57]) until now reporting phase diagrams for the SC polymer – LMM component systems of all three types are summarized in Table 1.

In the vast majority of cases, differential scanning calorimetry, cloud point determination and optical microscopy were used to construct the phase diagrams. Since these are kinetic methods, the results must be processed in order to gain thermodynamic characteristics of the system. In the case of DSC, the Hoffman – Weeks method was used [160] or data were extrapolated to the zero heating (or cooling) rate.[161]

Note that the DSC method was used not only to construct the liquidus line of the SC polymer identifiable with the melting curve of this polymer in the presence of the

Table 1. Semicrystalline polymer – LMM component systems for which phase diagrams are known and methods used to obtain data for constructing the phase diagrams.

No.	System	Methods of obtaining the data	Ref.
	Semicrystalline polymer – good solvent		
1	HDPE – xylene	Cloud point method	57
2	HDPE – *p*-xylene	DSC	61
3	HDPE – C_6 – C_{13} alkanes	Cloud point method	62
4	HDPE – phenyl methyl ether	Cloud point method	63
5	HDPE – liquid paraffin	DSC, optical microscopy	64
6	HDPE – mineral oil	DSC	65
7	UHMWPE – liquid paraffin	DSC, rheology	66, 67
8	LDPE – 1,3,5-trichlorobenzene	Cloud point method	68
9	LDPE – 3,6-dimethyloct-6-en-1-al	DSC, optical microscopy	69
10	Iso-PP – DOP	DSC, optical microscopy	70
11	Iso-PP – oleic acid	–	71
12	Iso-PP – mineral oil	DSC	65
13	Poly(4-methylpent-1-ene) – mineral oil	DSC	65
14	Poly(2,6-dimethyl-1,4-phenylene ether) – cyclohexanol	DSC, optical microscopy	72, 73
15	PVDF – sulfolane	DSC, optical microscopy	74
16	PVDF – diphenyl ketone	DSC, optical microscopy	75
17	PVDF – tributyl *O*-ethyl citrate	DSC, optical microscopy	76
18	PVDF – propylene carbonate	DSC	77
19	PVDF – DBP	DSC	65, 77, 78
20	PVDF – dibutyl sebacate	DSC	77
21	PVDF – γ-butyrolactone	DSC	77
22	PVDF – DEP	DSC, optical microscopy	79
23	PVDF – methyl 5-dimethylamino-2-methyl-5-oxopentanoate	DSC, cloud point method	80, 81
24	ECTFE – dioctyl adipate	DSC, cloud point method	82
25	Hexanediol polyadipate – toluene	DSC	83
26	Ethylene glycol polyadipate – dichloroethane	DSC	83
27	Ethylene glycol polysuccinate – methyldioxane	DSC	83
28	Decanediol polyadipate – 1,4-dioxane	DSC	83
29	Dodecanediol polyadipate – 1,4-dioxane	DSC	83
30	Copolymer of tetramethylene oxide with Nylon-12 – monophenyl ethylene glycol ether	DSC, optical microscopy	84
31	PLA – *N*,*N*-diethyl-3-methylbenzamide	DSC, optical microscopy	85
32	PLA – dioxane – water	DSC, cloud point method	86
33	PLA – chloroform – methanol	DSC, cloud point method	87

Table 1 (continued).

No.	System	Methods of obtaining the data	Ref.
	Semicrystalline polymer – poor solvent		
34	HDPE – DPE	Cloud point method	59, 63, 88 – 90
35	HDPE – amyl acetate	Cloud point method	57
36	HDPE – nitrobenzene	Cloud point method	57
37	HDPE – DOP/poly(tetramethylene glycol)	Optical microscopy	91
38	HDPE – soybean oil/poly(tetramethylene glycol)	Optical microscopy	91
39	HDPE – liquid paraffin/poly(tetramethylene glycol)	Optical microscopy	91
40	HDPE – soybean oil	DSC, optical microscopy	92
41	HDPE – DOP	DSC, optical microscopy	92
42	HDPE – soybean oil/DOP	DSC, optical microscopy	92
43	HDPE – diisodecyl phthalate	DSC, optical microscopy	93
44	HDPE – diisodecyl phthalate/dibenzylidene sorbitol	DSC, optical microscopy	94
45	HDPE – diphenyl	Cloud point method	63, 88
46	HDPE – (C_5 – C_{12}) aliphatic alcohols	Cloud point method	63
47	HDPE – *p*-*tert*-butylphenol	Cloud point method	63
48	HDPE – *p*-(1,1-dimethylpropyl)phenol	Cloud point method	63
49	HDPE – *p*-octylphenol	Cloud point method	63
50	HDPE – *p*-nonylphenol	Cloud point method	63
51	HDPE – *p*-phenylphenol	Cloud point method	63
52	HDPE – *o*-phenylphenol	Cloud point method	63
53	HDPE – *p*-benzylphenol	Cloud point method	63
54	HDPE – dibenzyl ether	Cloud point method	63
55	HDPE – benzyl phenyl ether	Cloud point method	63
56	HDPE – methyl phenyl ether	Cloud point method	63
57	HDPE – ethyl phenyl ether	Cloud point method	63
58	HDPE — β-naphthyl methyl ether	Cloud point method	63
59	HDPE – isopentyl acetate	Cloud point method	63
60	HDPE – benzyl propanoate	Cloud point method	63
61	HDPE – benzyl acetate	Cloud point method	63
62	HDPE – benzyl benzoate	Cloud point method	63
63	HDPE – cyclohexanone	Cloud point method	63
64	HDPE-grafted-maleic anhydride – di-n-octyl phthalate	DSC, cloud point method	95
65	HDPE/copolymer of ethylene with vinyl acetate – DPE	DSC, cloud point method	96
66	UHMWPE – DPE	DSC, optical microscopy	97
67	UHMWPE – decalin	DSC, optical microscopy	97
68	Iso-PP – myristic acid – diphenyl carbonate	DSC, optical microscopy	98
69	Iso-PP – tallowamine	DSC, cloud point method	99
70	Iso-PP – DBP/DOP	DSC, cloud point method	100
71	Iso-PP – DBP	DSC, optical microscopy	70, 101
72	Iso-PP – diamyl phthalate	DSC, optical microscopy	70
73	Iso-PP – dihexyl phthalate	DSC, optical microscopy	70
74	Iso-PP – dihepthyl phthalate	DSC, optical microscopy	70
75	Iso-PP – soybean oil	DSC, cloud point method	50, 102, 103
76	Iso-PP – soybean oil/DBP	DSC, optical microscopy	104, 105
77	Iso-PP – DPE	DSC, optical microscopy	48, 106
78	Iso-PP – soybean oil – carnauba wax	DSC, optical microscopy	107
79	sPP – dihexyl phthalate	DSC, optical microscopy	108
80	sPP – dihepthyl phthalate	DSC, optical microscopy	108
81	sPP – DOP	DSC, optical microscopy	108
82	sPP – dinonyl phthalate	DSC, optical microscopy	108
83	sPP – DPE	DSC, cloud point method	107, 109
84	Isotactic PS – cyclohexanol	DSC, cloud point method	110
85	EVOH – glycerol	DSC, optical microscopy	111
86	EVOH – poly(methyl methacrylate) – dimethylformamide	DSC, optical microscopy	112
87	Nylon-12 – PEG	DSC, optical microscopy	113
88	ECTFE – DBP	DSC, cloud point method	114
89	ECTFE – *N*-methylpyrrolidone	Cloud point method	115
90	ECTFE – DBP	DSC, cloud point method	116
91	ECTFE – DEP	DSC, optical microscopy	117
92	ECTFE – glycerol triacetate	DSC, optical microscopy	117
93	ECTFE – tributyl *O*-acetyl citrate	DSC, cloud point method	118

Table 1 (continued).

No.	System	Methods of obtaining the data	Ref.
	Semicrystalline polymer – poor solvent		
94	PVDF – glycerol triacetate/glycerol	DSC, optical microscopy	119
95	PVDF – dimethyl sulfone/glycerol	DSC, optical microscopy	120
96	PVDF – glycerol triacetate/glycerol	DSC, optical microscopy	121
97	PVDF – 1,2-propylene glycol	DSC, optical microscopy	122
98	PVDF – diphenyl ketone/1,2-propylene glycol	DSC, optical microscopy	122
99	PVDF – dimethyl phthalate	DSC, cloud point method	123
100	PVDF – dimethyl phthalate/dioctyl adipate	DSC, cloud point method	123
101	PVDF – diphenyl carbonate	DSC, optical microscopy	124
102	PVDF – γ-butyrolactone/DOP	Cloud point determination	125
103	PVDF – DBP/DOP	DSC, optical microscopy	126, 127
104	PVDF – dibutyl maleate	DSC, optical microscopy	128
105	Poly(phenylene sulfide) – diphenyl ketone	DSC, optical microscopy	129
106	Polytetrafluoroethylene – chlorotrifluoroethylene oligomer	DSC, cloud point method	130
107	PVF – benzmaleimide	Interferometry	131
108	PVF – dimethyl phthalate	Interferometry	131
109	PVF – DBP	Interferometry	131
110	PVF – dimethyl phthalate	Interferometry	131
111	PVF – dimethylphenylmaleimide	Interferometry	131
112	PVF – DOP	Interferometry	131
113	PVF – diphenyl phthalate	Interferometry	131
114	PVF – naphthylmaleimide	Interferometry	131
115	Polyacrylonitrile – dimethyl sulfone	DSC, optical microscopy, calculation	132
116	Cellulose acetate – dimethyl sulfone	DSC, optical microscopy, calculation	132
117	Cellulose diacetate – DEP	DSC	133
118	Poly{1-dimethylsilyl-4-[(dimethylsilylene)silyl]benzene} – bromobenzene	DSC	134
119	Poly{1-dimethylsilyl-4-[(dimethylsilylene)silyl]benzene} – 1-phenyldodecane	DSC	134
120	Copolymer of dimethylsiloxane with [(dimethylsilylene)phenylene-(dimethylsilylene)ethane-1,2-diyl] – *cis*-decalin	DSC	135
121	Copolymer of dimethylsiloxane with [(dimethylsilylene)phenylene (dimethylsilylene)ethane-1,2-diyl] – *trans*-decalin	DSC	135
122	Cellulose triacetate – nitromethane	Interferometry	136
	Semicrystalline polymer – crystalline compound		
123	HDPE – thymol	DSC	137
124	HDPE – camphor	DSC	137
125	HDPE – dimethyl terephthalate	DSC	137
126	HDPE – 1,2,4,5-tetrachlorobenzene	DSC	60, 137 – 139
127	HDPE – hexamethylbenzene	DSC	60, 137
128	Linear LDPE – pyrene	DSC	140
129	Iso-PP – 1,2,4,5-tetrachlorobenzene	DSC	141
130	Iso-PP – dotriacontane	DSC	142
131	Iso-PP – hexamethylbenzene	DSC	143
132	Iso-PP – camphene	DSC, optical microscopy	144
133	PEO – fenofibrate	Optical microscopy	145
134	PEO – flurbiprofen	Optical microscopy	145
135	PEO – $LiClO_4$	DSC	146
136	PEO – $LiCF_3SO_3$	DSC	146
137	PEO – $LiN(CF_3SO_2)_2$	DSC	146, 147
138	PEO – $KN(CF_3SO_2)_2$	DSC	147
139	PEO – $LiCF_3SO_2N(CH_2)_3OMe$	DSC	147
140	PEO – $KCF_3SO_2N(CH_2)_3OMe$	DSC	147
141	PEO – NaSCN	DSC, diffractometry	148
142	PEO – urea	DSC, optical microscopy	149, 150
143	PEO – *p*-hydroxybenzaldehyde	DSC	151
144	PEO – glutaric acid	DSC, optical microscopy	152
145	Poly(3-hexylthiophene) – methyl (6,6)-phenyl-C_{61}-butanoate	DSC	153, 154
146	Syndiotactic polystyrene – naphthalene	DSC, diffractometry	44
147	Poly(ε-caprolactone) – trioxane	DSC, optical microscopy	155
148	Nitrocellulose – glycerol triacetate	DSC	156

Table 1 (continued).

No.	System	Methods of obtaining the data	Ref.
	Semicrystalline polymer – crystalline compound		
149	PVDF – camphor	DSC, diffractometry	157, 158
150	Decanediol polyadipate – *p*-dichlorobenzene	DSC	83
151	Decanediol polyadipate – naphthalene	DSC	83
152	Dodecanediol polyadipate – *p*-dichlorobenzene	DSC	83
153	Dodecanediol polyadipate – naphthalene	DSC	83
154	Ethylene glycol polyadipate – *p*-dichlorobenzene	DSC	83
155	Ethylene glycol polyadipate – naphthalene	DSC	83
156	HDPE – ferrocene	Diffractometry	159

Note. The following designations are used: DSC is differential scanning calorimetry, UHMMPE is ultrahigh-molecular mass polyethylene, LDPE is low-density polyethylene, iso-PP is isotactic polypropylene, DOP is dioctyl phthalate, PVDF is poly(vinylidene fluoride), DBP is dibutyl phthalate, DEP is diethyl phthalate, ECTFE is ethylene copolymer with clorotrifluoroethylene, EVOH is ethylene copolymer with vinyl alcohol, PLA is polylactide, DPE is diphenyl ether, sPP is syndiotactic polypropylene, PEG is poly(ethylene glycol), PVF is poly(vinyl fluoride), PEO is poly(ethylene oxide), HDPE is high-density polyethylene; slash means that the solvent consisted of two components.

LMM component, but also to construct the temperature dependence of the solubility of the crystalline solid in the polymer. In most cases, the temperatures of endothermic (or exothermic) peak maxima were recorded; in some publications (see, for example, Refs 135, 158, 162), the DSC data were used to construct the Tammann plot for the enthalpy of the process as a function of the mixture composition. As a rule, the liquid – liquid binodal line was derived using optical methods (cloud point method,[57, 62, 63, 88, 95, 99] optical microscopy [64, 66, 91 – 94]).

A detailed review of methods used for studying phase equilibria is given in monographs by Chalykh and Gerasimov [1] and Vshivkov.[54] It was noted [54] that optical methods and DSC are used to construct the phase diagrams in more than 75% of cases. Mention should be made of the dynamic mechanical analysis method, which was also utilized [71, 163] to study the phase behaviour of mixtures of UHMMPE with liquid paraffin and PS with poly(vinyl methyl ether).

We will analyze some phase diagrams for the three types of systems presented in Table 1 in order to elucidate the general trends of the influence of experimental conditions and the natures and characteristics of the polymer and LMM component on the diagram topology and phase transition features upon the change of thermodynamic parameters of the system.

Typical examples of first type phase diagrams reflecting the existence of crystalline phase separation (Fig. 2)‡ were reported by Richards [57] and Berghmans *et al.*[72] for HDPE mixtures with xylene and poly(2,6-dimethyl-1,4-phenyl ether) with cyclohexanol. The liquidus line could not only have the shape discussed by Papkov [a sharp change in the melting temperature (T_m) in the highly polymer-lean domain; see Fig. 2 *a*], but can also show a monotonic decrease in the temperature with increasing content of the liquid in the mixture (see Fig.2 *b*, curve *1*). In some phase diagrams, the liquidus line of the polymer has a horizontal segment at high liquid contents.[71, 74]

The phase diagram shown in Fig. 2 *a* is based on the temperatures of disappearance of opacity in mixtures of different composition during heating. As noted above, line *2*

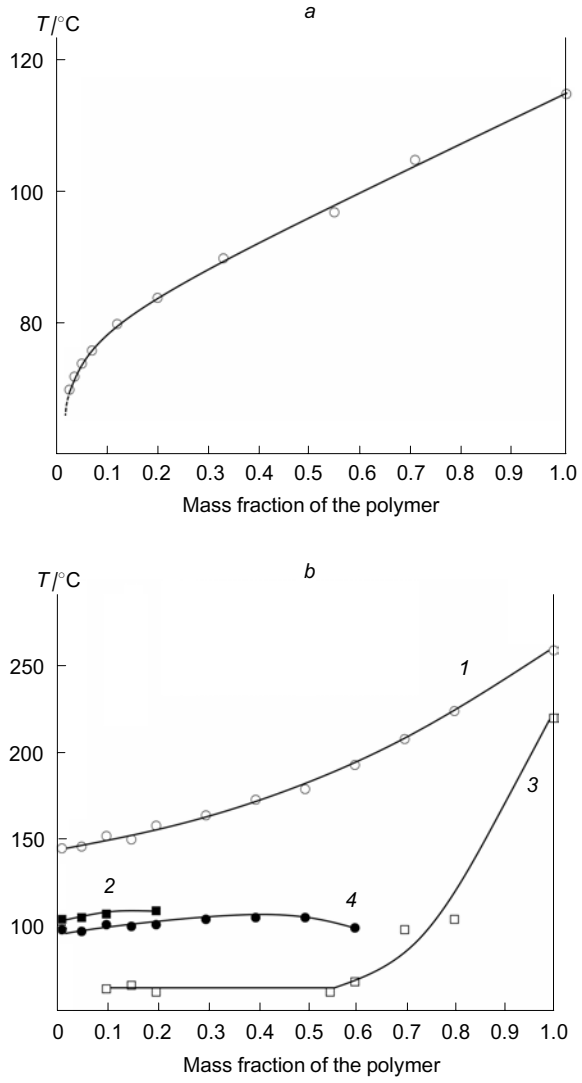


Figure 2. Phase diagrams of a LDPE mixture with xylene (*a*) [57] and a poly(2,6-dimethyl-1,4-phenyl ether) mixture with cyclohexanol (*b*).[72]
The dots in Fig. 2 *a* correspond to the temperatures of disappearance of opacity. In Fig. 2 *b*: points *1*, *3* and *4* are melting (DSC), glass transition and crystallization temperatures, respectively; points *2* are temperatures obtained by the cloud point method.

‡ Here and below the diagrams taken from original publications are presented in a more convenient form.

in Fig. 2 *b*, which is located between the DSC-based dependences $T_m(w_2)$ and $T_{cr}(w_2)$ (T_{cr} is the crystallization temperature, w_2 is the mass fraction of the polymer) is taken as a part of the liquid – liquid binodal line. Although this line can be detected only on cooling of a homogeneous mixture of the components rather than on heating, it is still considered as a phase separation curve that encompasses the coexistence domain of two liquid phases. This means that the system located above this binodal and below the $T_m(w_2)$ line constructed during cooling at a rate of 10 °C min^{-1} should exist in a nonequilibrium single phase state.

The dependence of the glass transition temperature (T_g) on the composition shown in Fig. 2 *b* is not a phase transition line, but it is rather useful for understanding the physical state of the polymer in the presence of various amounts of the liquid in the initial mixture of components.

The phase diagram of the PLA – *N*,*N*-diethyl-3-methylbenzamide system reported by Sungkapreecha *et al.*[85] is similar to that considered above: the liquid – liquid binodal is located considerably lower than the line reflecting the dependence of the crystallization temperature on the composition of the initial mixture. This arrangement of borderlines is due to the fact that the former was constructed for an amorphous polymer (L,D-PLA) and the latter was drawn for a semicrystalline polymer (L-PLA). However, while discussing the phase diagrams of this mixture, the authors did not pay due attention to the fact that these lines were obtained for different compounds.

The variation of the state of a homogeneous mixture of an SC polymer with a good solvent during cooling was described in detail by Lloyd *et al.*,[65] who considered the mechanism of membrane formation by the solid – liquid type thermally induced phase separation (TIPS). Crossing the liquidus line resulted in system separation into two phases: a solution of an amorphous polymer in the liquid and polymer crystallites. As the temperature decreased, the size of these crystallites increased and the concentration of the polymer solution decreased. This gave rise to a two-phase system in which the sphere-like particles of the SC polymer were distributed in the liquid (in the solution of the polymer in the LMM component). With decreasing content of the polymer in the initial mixture, the mass fraction of particles in the arising suspension regularly decreased.

An example of diagrams of the second type reflecting the phase equilibrium in a mixture of an SC polymer with a poor solvent is illustrated by Fig. 3. This mixture shows liquid – liquid and crystalline phase equilibria, with the domain of existence of the liquid – liquid equilibrium in the phase diagram being encompassed by two (see Fig. 3 *a*)[57] or one (the right one, see Fig. 3 *b*) binodal branches.[100] For a mixture of HDPE with nitrobenzene (see Fig. 3 *a*), the left- hand branch of the binodal virtually coincides with the ordinate axis.

The shift of the right-hand branch of the liquid – liquid binodal line for a mixture of iso-PP with the DBP – DOP mixed solvent downwards along the temperature axis with increasing content of DOP and degeneration of this branch for a polymer mixture with a pure DOP are illustrated by Fig. 3 *b*. This means that DOP is a good solvent for iso-PP. A similar shift of the binodal was observed by Chen *et al.*[105] upon the addition of soybean oil to DBP.

The interest in the phase equilibrium of SC polymer mixtures with mixed solvents is due to the desire to improve the performance of polymer membranes by changing the thermodynamic affinity of the components used to fabricate the membrane.[92, 94, 109, 104, 105, 123]

The position of the polymer liquidus line in the temperature – concentration field of the diagram (see Fig. 3 *b*) virtually does not depend on the co-solvent composition, but shifts to lower temperature with increasing cooling rate in the DSC experiment. Nevertheless, some researchers

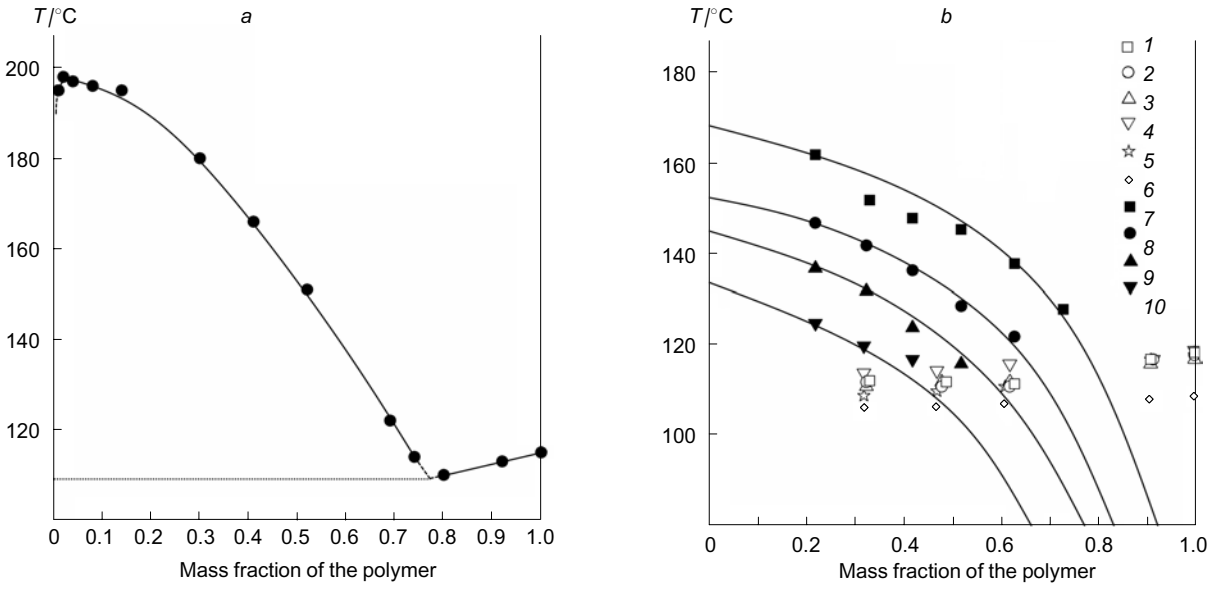


Figure 3. Phase diagrams of LDPE mixtures with nitrobenzene (*a*)[57] and iso-PP with DBP, DOP and their mixtures (*b*).[100]
The dots in Fig. 3 *a* correspond to the temperatures of formation of optically transparent homogeneous mixture; the dashed line shows the presumptive extension of the LDPE liquidus line. In Fig. 3 *b*, the open dots were obtained by the DSC method from the temperatures of the polymer crystallization peak at cooling rates of 5 (*1* – *5*) and 20 °C min^{-1} (*6*), the filled dots were obtained by the cloud point method. Mass fractions of DOP in the mixture with DBP: (*1*, *7*) 0.00, (*2*, *8*) 0.50, (*3*, *9*) 0.65, (*4*, *10*) 0.80, (*5*, *6*) 1.00.

discuss phase diagrams containing lines obtained by different methods at different temperature scanning rates.[85]

Mixtures of iso-PP with dialkyl phthalates exhibited [70, 109] a decrease in the UCST with increasing number of carbon atoms (from 4 to 10) in the alkyl substituent chain. An opposite trend was observed for mixtures of alkyl phthalates with polar PVDF: an increase in the UCST with elongation of the alkyl substituent. A study of mixtures of the same polymer with the DBP – DOP binary solvent [126] demonstrated that increasing the DBP fraction from 27.5 mass % to 32.5 mass % leads to a decrease in the UCST from 270 to 220 °C.

The dependence of the position of the liquid – liquid binodal line on the solvent molecular mass was studied [113] in relation to the polyamide-12 – PEG system. It was found that as the PEG molecular mass increases from 200 to 600, the UCST rises from 175 to 200 °C.

It was also ascertained [48, 93] that the liquid – liquid binodal line shifts upwards along the temperature axis with increasing molecular mass of the polymer, with the liquidus line position being virtually invariable. In particular, an increase in the molecular mass of iso-PP, when mixed with DPE, from 12 000 to 580 000 leads to an increase in the UCST from 110 to 135 °C.[48]

The effect of the polymer structure on phase diagrams is well demonstrated in a study of Yave *et al.*[106] It was shown that on going from isotactic to syndiotactic PP mixed with DPE, the liquidus line of the polymer shifts to lower temperature, while the UCST increases.

Shang *et al.*[111] used DSC and cloud point measurements to study the phase equilibrium in mixtures of glycerol with EVOH. It was found that the liquid – liquid binodal line shifts downwards along the temperature axis as the mole fraction of ethylene in the copolymer decreases from 0.44 to 0.38. Conversely, the crystallization temperature of the copolymer increases and finally (when the ethylene mole fraction is 0.32) becomes above the binodal temperature.

The sequence of transitions involved in the thermally induced phase separation of the homogeneous SC polymer – poor solvent system is described in detail by Lloyd *et al.*[99]

Like in the case of cooling of a homogeneous system comprising an SC polymer and a good solvent, crossing the liquidus line located on the right from the so-called monotectic point is followed by polymer crystallization. This gives rise to the two-phase system composed of polymer crystallites and a polymer solution in the liquid; as the temperature decreases, the solution composition varies according to the law specified by the liquidus line. When this phase reaches the composition corresponding to the monotectic point, liquid – liquid phase separation takes place. The polymer-lean droplets are entrapped within the spherulites and the system becomes a three-phase one. However, the researchers do not discuss whether or not the three-phase state of the system is retained on further cooling.[99]

Cooling of the homogeneous system located on the left from the monotectic point down to the liquid – liquid binodal induces separation of the system into two liquid phases, the compositions of which is specified by positions of the left- and right-hand branches of the binodal. The morphology of the arising two-phase system depends on the ratio between the composition of the initial mixture (w_2) and the composition corresponding to the upper critical solution temperature (w_{2UCST}). When $w_2 < w_{2UCST}$, a dispersion of droplets of the polymer-rich phase in the polymer-lean phase is formed. When $w_2 \approx w_{2UCST}$, an interpenetrating phase structure appears, while when $w_2 > w_{2UCST}$, the polymer-lean phase is dispersed as droplets in the polymer-rich phase. Further cooling to a temperature below the monotectic point induces polymer crystallization from the polymer-rich phase, and a three-phase system thus appears.

The phase diagrams of the HDPE – TCB,[60] HDPE – dimethyl terephthalate (DMTP) [137] and HDPE – thymol [137] systems constructed by the DSC method are shown in Fig. 4.

In a system characterized by the phase diagram shown in Fig. 4 *a*, the melting point of the LMM component is above the polymer melting temperature. The phase diagram of this system is considered to be the full analogue of the diagram for a mixture of two crystallizable LMM liquids. It can be seen that the eutectic composition is shifted towards the axis corresponding to the lower melting point component. Diagrams of this type were obtained for mixtures of HDPE with camphor,[137] HMB [60, 137] and ferrocene;[159] iso-PP with hexamethylbenzene [143] and TCB;[141] poly(ε-caprolactone) with trioxane;[155] PEG with glutaric acid,[152] fenofibrate,[145] flurbiprofen [145] and *p*-hydroxybenzaldehyde;[151] and poly(3-

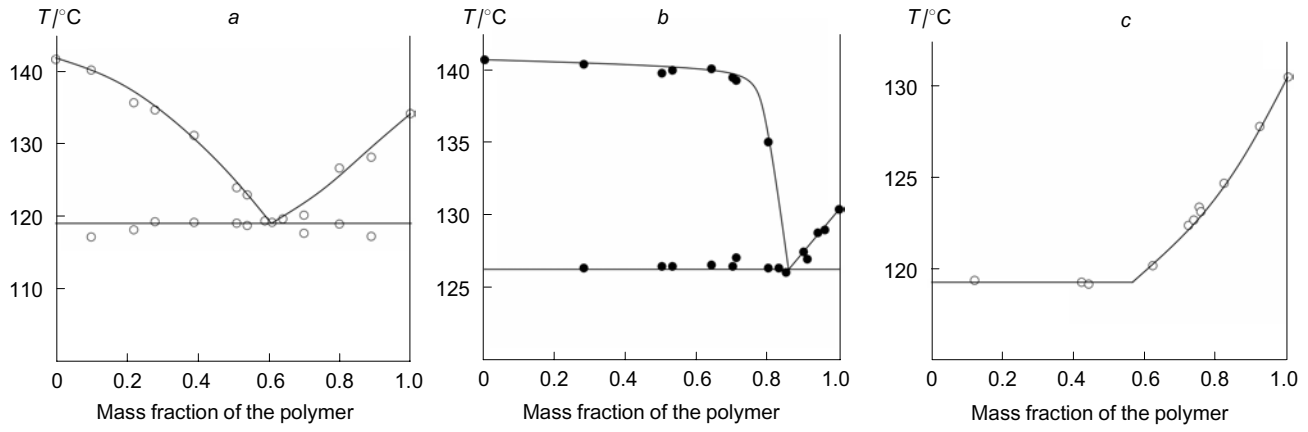


Figure 4. Phase diagrams of mixtures: HDPE with TCB (*a*),[60] HDPE with DMTP (*b*) [137] and HDPE with thymol (*c*).[137]

hexylthiophene-2,5-diyl) with methyl 6,6-phenyl-C_{61}-butyrate.[153]

A sort of diagram of this type is the phase diagram of an HDPE – DMTP mixture[137] constructed using DSC data at a heating rate of 5 °C min^{-1} (Fig. 4 *b*). This diagram has an almost horizontal segment corresponding to the DMTP melting point. It was shown that a homogeneous molecular mixture of the components is formed at a significantly higher temperature; the dependence of this temperature on composition was not studied. It was assumed that above the horizontal segment, there is a domain bounded by the liquid – liquid binodal line in which two liquid phases coexist. This type of diagram, combining features of the diagrams shown in Figs 1 *b* and *c*, was predicted by calculations in terms of the Flory theory.[164]

The phase diagram of the HDPE – thymol system, in which the melting point of the LMM component is ~80 °C lower than that of the polymer, is presented in Fig. 4 *c*.[137] Since thymol is liquid in the relevant temperature range, the diagram is similar to the diagrams obtained for mixtures of SC polymers with good solvents. However, the solubility in the domain above the horizontal segment of the liquidus line was not studied in detail and DSC measurements did not show any thermal effects in this domain; hence, the question of whether thymol is a good or poor solvent for HDPE remains open.

Smith and Pennings[60] reported the phase diagram of the HDPE – HMB system with an isotherm located ~10 °C below the solidus line within the $0 < \varphi_2 < 0.8$ range where φ_2 is the volume fraction of the polymer in the mixture. In the authors' opinion, this isotherm corresponds to the solid – solid phase transition, which reflects the polymorphic transformation of hexamethylbenzene crystals that same was also detected in another study.[165]

An effect of the polymer molecular mass on the position of the dependence $T_{cr}(w_2)$ was detected only in a study of phase equilibrium in mixtures of PEG with fenofibrate and flurbiprofen.[145] It was shown that with increasing polymer molecular mass from 3 500 to 20 000, this dependence slightly (by ~5 °C) shifts to higher temperature.

Studies of the phase equilibria in polymer mixtures with LMM compounds involving formation of crystalline complexes (clathrates, intercalates and so on) demonstrated[44, 146 – 148, 157, 158] that the phase diagrams for mixtures of syndiotactic polystyrene (PS) with naphthalene and mixtures of PEO with urea or organic and inorganic salts are more sophisticated because of the presence of coexisting domains of crystalline complexes with different stoichiometry.

Studying the effect of the annealing temperature on the position of borderlines in the phase diagram of a mixture of HDPE with TCB showed that lowering the temperature at which the sample was kept after cooling from the homogeneous state is accompanied by displacement of the polymer liquidus towards lower temperature and displacement of the eutectic point towards polymer-rich mixtures.[139]

The behaviour of a homogeneous mixture of an SC polymer with a crystalline LMM compound with the melting point close to that of the polymer on lowering the temperature is described in the following way. Cooling of an eutectic mixture leads to simultaneous crystallization of the components, while cooling of a mixture of any other composition induces crystallization of the component the amount of which in the initial mixture is higher than that in the eutectic one. When the eutectic composition is attained, the mixture crystallizes over a short period of time.[139] According to Alwatarri and Lloyd,[143] crystallization of the LMM component also takes place in mixtures containing a somewhat lower amount of this component than the eutectic mixture, while in the case of considerably polymer-rich mixtures, the polymer is the first to crystallize and then the separation of the LMM as droplets and crystallization in the droplets take place simultaneously. According to Alwatarri and Lloyd,[143] this is due to the pronounced difference between the crystallization rates of low- and high-molecular-mass compounds. In our opinion, these views are not quite correct, because they are based on the scanning electronic microscopy data for the samples obtained at room temperature, which is much lower than the crystallization temperature.

The gelation problem also deserves mention. The issues concerning the phenomenology of formation and estimation of physicomechanical, thermal and other properties of polymer gels are actively discussed in the literature.[44, 65, 76, 84, 99, 166, 167] However, only few publications are devoted to identification of the temperature – concentration domain of phase diagrams in which single-phase thermally reversible two-component gels based on SC polymers may exist.[76, 84, 166, 167]

An original approach has been proposed[161] consisting in determining the temperature at which a metallic ball placed on the surface of a pre-homogenized LDPE mixture with various alkylbenzenes (toluene, *o*-xylene, benzene) that was cooled down to room temperature in a sealed tube started to be immersed into the mixture on heating under the action of gravity. The results of measurements were used to construct two borderlines in the phase diagram, one of which (vertical) corresponds to the minimum polymer content in the solution sufficient for gelation, while the other one reflects the dependence of the gel melting temperature on the initial mixture composition. It is obvious that in the physical meaning, the second borderline is close to the liquidus line.

Guenet and co-workers[167] identified the liquidus line constructed using DSC with the sol – gel transition boundary. In the authors' opinion, the former of the above-noted lines corresponds to the boundary that separates the polymer solution in the liquid from the liquid solution in the polymer and is shifted towards polymer-rich compositions.

For constructing the borderline reflecting the sol – gel transition, Cui *et al.*[76] proposed a procedure based on determination of the lowest temperature at which the gravity-induced flow of a homogenized mixture of a PVDF melt with tributyl *O*-acetyl citrate was still observed as the tube was turned upside down. The curve obtained by this procedure in the $0.1 < w_2 < 0.35$ range of compositions is located somewhat lower than the liquidus line constructed using the DSC data.

Generally, in the context of traditional views on the phase equilibrium in the SC polymer – LMM component systems, the domain of gel existence can be identified only approximately. It is clear even from purely geometric reasons that at least one more curve is required for the strict definition of the boundaries of this domain.

Thus, according to traditional views, the SC polymer is considered as a single-phase crystalline system, a set of defective crystals containing amorphous and crystalline regions. It is assumed that the phase equilibrium in a mixture of an SC polymer with an LMM component obeys the Gibbs phase rule and does not differ conceptually from

the equilibrium in a mixture of two crystallizable LMM compounds. The specificity of the SC polymer – thermodynamically good solvent system is reduced to the existence of only one phase line in the diagram, namely, the dependence of the polymer melting temperature on the composition of the initial mixture, which reflects the crystalline phase equilibrium. A specific feature of the SC polymer – poor solvent system is the appearance of the liquid – liquid binodal phase separation above the horizontal segment of the liquidus line of the polymer component. The combination of these two curves reflects the existence of the liquid – liquid and crystalline phase equilibria in the system. The phase diagram of the SC polymer – crystalline LMM compound system is interpreted as a full analogue of the fusion diagram of a mixture of two crystalline LMM compounds containing an eutectic point, which reflects the co-existence of three phases — crystals of both components and their liquid mixture.

The position of the borderlines in the phase diagram depends on the polymer nature, molecular mass and thermal prehistory and low-molecular-mass compound structure and molecular mass. A general trend that can be followed for the SC polymer – LMM component systems listed in Table 1 is the dependence of the positions of borderlines and monotectic and eutectic points on the temperature scan rate. The diagrams constructed by means of kinetic methods are not equilibrium; however, they are used for discussion of phase equilibria and phase transitions. Considering the fact that lines reflecting the dependences of the glass transition, flow and sol – gel transition temperatures on the mixture composition can also be put on the temperature – concentration fields of the diagrams, it is more appropriate to call them diagrams of the state of mixtures rather than phase diagrams.

Virtually all SC polymer – LMM component systems form single-phase thermoreversible gels, but the corresponding domain is not reflected in the phase diagrams. The interpretation of the evolution of the phase structure during the thermally induced phase separation of a homogeneous mixture proposed in the literature does not provide a correct description of the mechanism of formation of capillary porous bodies (membranes, granules, *etc.*).[1] It should be emphasized that the phase diagrams obtained by different authors under roughly the same conditions of kinetic experiments do not always agree with one another. This lack of agreement is illustrated by reported phase diagrams of PVDF and DBP mixtures.[77, 78]

3. New description of a phase equilibrium

Mizerovskii *et al.*[168] were the first to formulate the view that, according to macroscopic thermodynamics, SC polymers are single-phase liquids with the following specific features:

— SC polymers are clearly and steadily heterogeneous at the microlevel, but they are homogeneous as Gibbs macrophases, since structural parameters of macroscopic samples of any size are equal;

— due to incomplete crystallization of elementary units of macromolecules, the SC polymers are thermodynamically non-equilibrium and, because of physical indivisibility (without destruction) of microvolumes with different degrees of ordering of the spatial arrangement of elementary units, they are internally strained;

— from the structural standpoint, they are cross-linked polymer networks with thermotropic cross-links represented by crystallites; unlike in vulcanized elastomers (which are also 3D-structured liquids), the volumes of cross-links and regions between them in SC polymers are comparable.

Thus, SC polymers are single-phase internally stressed (metastable) spatially structured (microheterogeneous) liquids with crystallites functioning as the cross-links of the intrmolecular bond network.

A liquid phase of this type has three specific features. First, because of molecular inhomogeneity (polydispersity), inherent in most polymers, this phase is actually multicomponent.[7, 169 – 171] Second, in terms of the classical theory of polymer solutions,[7] it is characterized by 'component dualism': the whole macromolecules act as components of the polymer liquid with respect to the LMM component as a phase, since they participate in the phase exchange; however, segments of macromolecules act as components of the polymer liquid with respect to the LMM molecules that have passed to the polymer liquid phase. Third, the transfer of macromolecules to the LMM liquid phase is possible only after they acquire translational mobility, which occurs after all crystallites disappear.

In terms of this approach, Mizerovskii *et al.*[168] gave a detailed substantiation for the necessary presence of one more borderline in all phase diagrams. This line can be interpreted as either the temperature dependence of the solubility of the LMM component in the amorphous regions of the SC polymer or as the temperature boundary of transformation of the initial two-phase system comprising the SC polymer and the LMM component into a single-phase system, a solution of the LMM component in the SC polymer.

The first studies devoted to swelling of SC polymers in low-molecular-mass liquids appeared in the mid-20th century.[172, 173] The experimentally determined swelling ratios proved to be lower than the values calculated using the Flory – Huggins theory, even if the impermeability of crystallites for the LMM liquid is taken into account. Two approaches were proposed to address this issue. According to the first one, based on the Flory – Rehner theory developed for vulcanized rubbers, it is assumed that crystallites function as giant cross-links.[172] The second approach uses the view that the tie chains connecting crystallites are strained at temperatures below the polymer melting temperature where the free energy of elastic deformation is equal to the free energy of crystallization.[173] According to calculations,[174 – 176] strained, or elastically effective chains account for $\geqslant 30\%$ of the total mass of the amorphous polymer. The rest of the material is represented by non-crystallized short chains, loops, folds and free ends that do not undergo elastic deformation during sorption of the LMM component.

Subsequently, these views were upgraded[174 – 178] by introducing an additional parameter into the Flory – Huggins and group contribution theories to take into account the free energy of elastic deformation of tie chains. As a result, the researchers obtained dependences of the solubilities of low-molecular-mass compounds in polyethylene and polypropylene on their activity at various temperatures[174, 175] and temperature dependences of the partition coefficient[176] and found the proportions of elastically effective tie chains. The calculations carried out with allow-

ance for these relationships are in good agreement with experimental data for SC polymers.

Meanwhile, none of the cited publications report an explicit equation suitable for describing the temperature dependence of the LMM component solubility in the SC polymer.

The above approach is in line with the idea stated by Mizerovskii *et al.*[168] based on the views of Alfrey and Mark,[179] according to which the tie chains are strained due to low entropy; therefore, crystallites involving these chains are strained. From the physical standpoint, this means that under ambient conditions in the absence or in the presence of a liquid, the polymer crystallites grow being subjected to uniform extension strain, with a force increasing with increasing average degree of crystallinity and with decreasing length of the tie chains.

In this situation, the highest possible degree of crystallinity of the polymer is dictated by thermomechanical rather than thermodynamic equilibrium conditions, which, in a first approximation, can be formulated as follows: in any microvolume of an SC polymer, the internal strain of the amorphous regions is equal to the ultimate strain upon the uniform extension of the most defective crystallites.[168] It was shown in the same study that the addition of the solubility curve changes the thermodynamic meaning of the phase diagram, since it separates two- and single-phase domains. This curve is also present in the diagrams drawn by Chalykh *et al.*,[131] who regarded it as reflecting the 'solubility in the amorphous region of the polymer' and did not use it for analysis of the phase structure of a binary mixture.

Pochivalov and co-workers[180–196] constructed phase diagrams for polyolefin mixtures with various low-molecular-mass components (good or poor solvents, crystalline compounds) containing the solubility curve for the low-molecular-mass component in the SC polymer. The data on these studies are summarized in Table 2.

The diagrams were constructed using four methods: optical,[180–195] DSC,[181,184–191,193–196] gravimetric[180] and cloud point measurement.[196]

The optical method consists in observation, using a horizontal microscope, of changes in the state of a closed polymer – LMM component system during stepwise temperature variation. The method is based on the difference between the refractive indices of coexisting phases; the temperature at which the state of a two-phase system qualitatively changes on heating can thus be determined with an accuracy of ± 0.5 °C.

The DSC curves of mixtures of SC polymers with LMM components during heating, cooling and repeated heating were measured on Phoenix NETZSCH 204F1 and Mettler-Toledo DSC 823e/400 calorimeters at a heating rate of 10 °C min^{-1}.

The experimental procedure involved in the cloud point method was as follows. The mixtures pre-homogenized at elevated temperature for at least 5 h were cooled to room temperature at a rate of 10 °C min^{-1} in sealed glass tubes placed in a special thermostat. The phase separation temperature was detected as the onset of sample opacity.

Before the experiments, SC polymer granules were, most often, treated with an excess of the LMM component below the amorphization temperature to extract fractions of macromolecules with a low molecular mass, which do not participate in the formation of crystallites. This treatment was not carried out in two cases, first, to study SC polymer mixtures with a crystalline LMM compound and, second, to study an LDPE – decane mixture. Apart from the optical method, the gravimetric method, that is, determination of the mass of macromolecules that pass to the solvent phase upon extraction, was used to construct the phase diagram of the last-mentioned system.

Pochivalov and co-workers[180–188] describe the phase behaviour of SC polymer mixtures with a good solvent (the first type according to our classification). Figure 5 presents

Table 2. Semicrystalline polymer mixtures with the low-molecular-mass component for which phase diagrams were constructed in the context of new interpretation of phase equilibria.

No.	System	Methods of obtaining the data	Ref.
	Semicrystalline polymer – good solvent		
1	LDPE – decane	Optical, gravimetric	180
2	LDPE – tridecane	Optical	180
3	LDPE – toluene	Optical, DSC	181
4	LDPE – *o*-xylene	Optical	182
5	LDPE – *p*-xylene	Optical, DSC	183, 184
6	LDPE – *m*-xylene	Optical, DSC	183
7	LDPE – ethylbenzene	Optical	182
8	LDPE – mineral oil	Optical, DSC	185
9	HDPE – *m*-xylene	Optical, DSC	186
10	Iso-PP – *m*-xylene	Optical, DSC	187
11	PBAMO – ternary mixture of dinitrodiiazaalkanes	Optical, DSC	188
	Semicrystalline polymer – poor solvent		
12	Iso-PP – DBP	Optical, DSC	189, 190
	Semicrystalline polymer – crystalline compound		
13	LDPE – 1,2,4,5-tetrachlorobenzene	Optical, DSC	191
14	HDPE – 1,2,4,5-tetrachlorobenzene	Optical, DSC	191 – 193
15	Iso-PP – 1,2,4,5-tetrachlorobenzene	Optical, DSC	191, 194
16	Poly[3,3-bis(azidomethyloxetane) – 2,4-dinitro-2,4-diazapentane]	Optical, DSC	195
17	LDPE – thymol	Optical, DSC, cloud point method	196

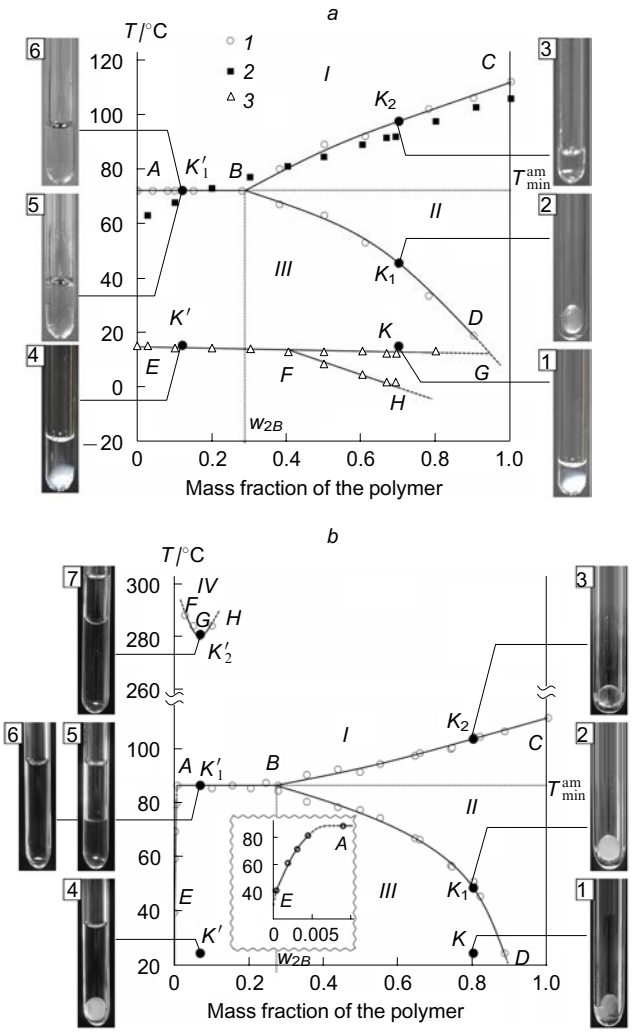


Figure 5. Phase diagrams of LDPE mixtures with *p*-xylene (*a*) [184] and with n-decane (*b*) [180] supplemented by photographs (1 – 7), which illustrate the state of the mixtures at different points of the temperature – concentration field (for explanations, see the text). (*1*) Data of the optical method, (*2*) maxima of high-temperature endothermic peaks, (*3*) maxima of low-temperature endothermic peaks.

the phase diagrams for the LDPE mixtures with *p*-xylene [184] and n-decane.[180] In the polymer-rich domain of the former mixture, the optical method makes it possible to detect two events during heating of the initial two-phase polymer – liquid system starting from 15 °C:

(**1**) disappearance of the low-molecular-mass liquid *via* dissolution in the polymer, which remains opaque and swells;

(**2**) transformation of the swollen polymer into optically transparent liquid.

In the LMM-component-rich region, heating is also accompanied by two events, which successively take place at the same temperature:

(**3**) formation of an optically transparent two-phase system with a clear-cut interface;

(**4**) transformation of this two-phase system into a single-phase one upon mixing.

In the phase diagram shown in Fig. 5 *a*, the borderlines *BD*, *BC* and *AB* are constructed using the temperatures that correspond to events **1**, **2** and **3**, **4** for mixtures of different compositions. This Figure also shows photographic images, which demonstrate the state of the system at 15 °C and at temperatures of the indicated events.

It can be seen that at 15 °C (point *K* in Fig. 5 *a*), LDPE granule and transparent *p*-xylene coexist in the initial mixture containing 0.7 mass fractions of the polymer (photo 1). During stepwise heating of this two-phase system, the size of the polymer granule gradually increases, while the amount of the transparent liquid phase simultaneously decreases. Photo 2 depicts the situation corresponding to event **1** when the transparent liquid completely disappears being dissolved in the polymer (point K_1 in Fig. 5 *a*). As the temperature is further increased, the opacity of the swollen granule decreases, and at the temperature corresponding to point K_2 on line *BC*, the polymer is completely amorphized, becomes transparent and flows under gravity, taking the shape of the tube (photo 3), which corresponds to event **2**.

With excess *p*-xylene ($w_2 = 0.1$), the state of the system at point K' in Fig. 5 *a* is the same as at point *K* (photo 4). On the way from K' to K'_1 the polymer granule coexisting with transparent liquid grows and its opacity decreases. When the temperature of point K'_1 in line *AB* is attained, event **3** corresponding to the formation of an optically transparent two-phase liquid system takes place (photo 5). After ~10 h at the same temperature, the two-phase system is transformed into a single-phase homogeneous liquid (event **4**, photo 6). A similar behaviour at this temperature was found for all mixtures at $w_2 < w_{2B}$.

Thus, during heating of a mixture with $w_2 > 0.28$ (see Fig. 5 *a*), the formation of an optically transparent molecular mixture of the polymer and the liquid is preceded by the formation of the single-phase opaque microheterogeneous system (a solution of the LMM liquid in the SC polymer). In other words, heating of this system results in complete amorphization of LDPE, with the destruction § of the polymer crystallites on the way from point *K* to point K_1 being caused by both dissolution of *p*-xylene in the polymer and by temperature rise, while that on the way from K_1 to K_2 is due only to the temperature rise.

Heating of the mixture corresponding to the condition $w_2 < w_{2B}$ gives rise to a molecular mixture of a polymer melt and a liquid at 72 °C (point K'_1), which is preceded by the formation of a two-phase optically transparent system. If $w_2 = w_{2B}$, the initial two-phase system directly turns into an optically transparent homogeneous mixture of components at point *B* (see Fig. 5 *a*). This means that figurative point *B* characterizes the lowest temperature of complete amorphization of the polymer ($T^{\mathrm{am}}_{\mathrm{min}}$) that can be reached upon dissolution of $(1 - w_{2B})$ mass fractions of a liquid in the polymer. When $w_2 < w_{2B}$, the two-phase system arising at $T^{\mathrm{am}}_{\mathrm{min}}$ is a solution of the liquid in the polymer containing $(1 - w_{2B})$ mass fractions of this liquid and an excess of pure liquid (without pretreatment of polymer granules, this liquid would have contained dissolved polymer fractions not participating in the formation of crystallites). The behaviour of this two-phase system depends on the relation-

§ By the term 'destruction of crystallites' is meant that the gradual change in the degree of crystallinity of the polymer with increasing temperature is a reversible thermomechanical process both in the presence and in the absence of the liquid.[190] Only the last crystallites not interconnected by tie chains undergo thermal destruction (melting).

ship between T_{min}^{am} and the upper critical solution temperatures of the system components. If T_{min}^{am} is lower than the UCST, a liquid – liquid binodal, reflecting the temperature boundary of mixture homogenization, would appear in the diagram. If T_{min}^{am} is greater than or equal to the UCST, then any two-phase system containing more than $(1-w_{2B})$ mass fractions of the liquid would be spontaneously transformed into a molecular mixture of the polymer and the liquid at T_{min}^{am}. In the LDPE – *p*-xylene system, the latter situation takes place, giving rise to horizontal segment *AB* (see Fig. 5 *a*).

The borderlines *ABC* and *ABD* based on optical data have the following thermodynamic meaning. Line *ABC* reflects the variation of the melting temperature of the last polymer crystallites not connected by tie chains as a function of the amount of the LMM component present in the initial system. Line *ABD* corresponds to the temperature boundary of transformation of the initial two-phase system into a single-phase one, namely, into a molecular mixture of an LDPE melt and *p*-xylene in segment *AB* and into a solution of *p*-xylene in amorphous regions of solid LDPE in segment *BD*. Below this line, pure *p*-xylene coexists with its solution in the amorphous regions of LDPE. The temperature dependence of the composition of the second phase is described by segment *BD*. In the domain below this line, unidirectional diffusion of small *p*-xylene molecules towards the polymer bulk takes place and osmotic equilibrium is established, with the polymer serving as the osmotic cell. In this situation, polymer is the solvent and the LMM component is the solute.

Since the osmotic equilibrium is not a phase equilibrium in the classical meaning of this term,[3] segment *BD* reflecting the *p*-xylene solubility in LDPE is not a phase coexistence line.

Line *ABC* coincides with *ABD* in segement *AB,* which is typical of SC polymer – good solvent systems for which the UCST, as noted above, is lower than or equal to T_{min}^{am}. Crossing line *BC* reflects the change in the physical state of the polymer component in a single-phase system and is accompanied by a heat effect due to disappearance (on heating) or appearance (on cooling) of LDPE crystallites that are not already (or not yet) bound by tie chains. According to our interpretation, this crossing does not change the number of phases in the system (except that at point *B*), but results in the appearance or disappearance of microheterogeneity inside the macroscopic phase. The presence of heat effect indicates that this process can be regarded as a first order phase transition, but only relative to the segments of macromolecules rather than the whole macromolecules as mixture components.

Segment *BC* divides the single-phase domain located above line *ABD* into two subdomains. Above line *BC*, there are molecular mixtures of LDPE melt with *p*-xylene, while below line *BC*, there exist *p*-xylene solutions in amorphous regions of LDPE, which are in essence thermoreversible single-phase gels. The crystallites connected by tie chains serve as the cross-links of this gel, with the mass fraction of the crystallites (the degree of polymer crystallinity) decreases on heating of the mixture of a definite composition and becomes equal to zero as segment *BC* is reached. The degree of crystallinity also increases with increasing LDPE content in the system at an invariable temperature up to the value corresponding to the pure polymer.

Thus, curves *ABC* and *ABD* form three domains in the phase diagram:

domain *I* corresponds to a single-phase molecular mixture of *p*-xylene with LDPE melt;

domain *II* corresponds to a single-phase thermoreversible physical gel, that is, a solution of *p*-xylene in the amorphous domains of LDPE;

domain *III* corresponds to a two-phase mixture of pure *p*-xylene and its solution in LDPE (gel), which exist in osmotic equilibrium.

Phase diagrams such as those shown in Fig. 5 *a* were constructed [180 – 187] for LDPE mixtures with toluene, *o*- and *m*-xylene, ethylbenzene, n-decane, n-tridecane and mineral oil and for mixtures of HDPE and iso-PP with *m*-xylene. Analysis of these diagrams showed that the position of figurative point *B* is an important thermodynamic characteristic of the SC polymer – LMM liquid system. In particular, the thermodynamic affinity level of the components can be estimated using parameters related to the position of point *B* such as the ratio $\beta = T_{min}^{am}/T_m$ and the difference $1-w_2$.[182, 189] The former characterizes the most pronounced decrease in the temperature of complete polymer amorphization upon dissolution of the particular LMM liquid in the polymer, while the latter characterizes the minimum mass fraction of the liquid in the initial mixture that is sufficient for attaining T_{min}^{am}. The values of these characteristics for the given LDPE mixture with alkylbenzenes are summarized in Table 3.

Table 3. Thermodynamic parameters of the LDPE – alkylbenzene systems calculated from the position of figurative point *B*.

System	T_{min}^{am} /°C	β	$1-w_{2B}$	Ref.
LDPE – toluene	68	0.61	0.90	181
LDPE – *o*-xylene	68	0.61	0.78	182
LDPE – *m*-xylene	69	0.62	0.75	183
LDPE – *p*-xylene	72	0.64	0.72	183
LDPE – ethylbenzene	73	0.65	0.68	182

The fact that the mutual solubility of components increases with decrease in the former and increase in the latter characteristics indicates that the thermodynamic affinity of solvents to LDPE increases in the order

ethylbenzene < *p*-xylene < *m-xylene* < *o*-xylene < toluene

For comparison, Table 4 shows the Hildebrand solubility parameters (δ) for the LMM liquids found using experimental data from the known relation [197, 198]

$$\delta = \sqrt{\frac{\Delta H_V - RT}{V_\mu}} \quad (1)$$

Table 4. Hildebrand solubility parameter of alkylbenzenes calculated from experimental data and by the group contribution method.[197 – 200]

Name	Calculation of $\delta \times 10^3$ /(J m^{-3})$^{0.5}$	
	from experimental data	by the group contribution method
Toluene	17.2	18.1
o-Xylene	17.4	17.8
m-Xylene	17.1	17.8
p-Xylene	16.9	17.8
Ethylbenzene	16.8	17.8
LDPE	16.8	16.2

where ΔH_V is the molar heat of vaporization of the liquid, V_μ is the molar volume of the liquid; the δ values presented for LDPE were recommended in a book [199] and calculated by the group contribution method.[200] It is assumed that the smaller the difference between the solubility parameters of compounds the higher their mutual solubility. Hence, considering the experimental data, the LDPE affinity of LMM liquids should increase in the order

o-xylene < toluene < *m*-xylene < *p*-xylene < ethylbenzene

while the group contribution method predicts the order

toluene < *o*-xylene = *m*-xylene = *p*-xylene = ethylbenzene

A possible cause for the discrepancy may be the fact that the data of Table 3 refer to the $T_{\min}^{\text{am}} < T < T_{\text{m}}$ temperature range in which LDPE, in the presence of the given LMM compound, is completely amorphized (in all cases, $T_{\min}^{\text{am}} \approx 70$ °C), while the data of Table 4 refer to room temperature where the polymer crystallinity should play an important role.

The generalized phase diagram of an LDPE mixture with n-decane, which has been never studied before, is depicted in Fig. 5*b*. The diagrams for HDPE mixtures with n-alkanes available from the literature [62] are fragmentary, as they contain only liquid – liquid binodals with the lower critical solution temperature (LCST) above the boiling point of the LMM liquid. The optical method we used makes it possible to identify the above-described events **1** and **2** during heating of polymer-rich mixtures. For LMM component-rich compositions, event **5**, reflecting the separation of the formed homogeneous mixture into two transparent macrophases, is observed apart from events **3** and **4**. It is noteworthy that events **3** and **4** take place at the same temperature, while event **5** occurs at a higher temperature.

Prior to the experiment,[180] the LDPE granules were not treated in a large volume of the solvent to remove non-crystallized macromolecules possessing translational mobility. Therefore, there was a good reason to believe that during the stepwise heating of the mixture from room temperature to event **3** at $T_{\min}^{\text{am}}$, these macromolecules are extracted from the solid SC polymer into the solvent phase to give a polymer solution in the liquid. The mass of macromolecules extracted in the temperature range of 40 – 80 °C was determined by the gravimetric method.[180]

The phase diagram shown in Fig. 5*b* contains four borderlines — *FGH*, *ABC*, *ABD* and *EA*. Lines *BD*, *BC*, *AB* and *FGH* correspond to the temperatures of events **1**, **2**, **3** and **4**, **5**, respectively. Curve *EA* was constructed using gravimetric data.

Comparison of the photographs presented in Fig. 5*a*,*b* indicates that the processes and events taking place in the LDPE – *p*-xylene and LDPE – n-decane systems are similar. The difference is that in the latter case at $w_2 < w_{2B}$, the optically transparent system that has formed at $T_{\min}^{\text{am}} = 87$ °C after ~15 h of observation (photo 6 in Fig. 5*b*) is separated into two phases at a higher temperature (photo 7).

Line *FGH* in Fig. 5*b* reflects the existence of liquid – liquid equilibrium with a lower critical solution temperature. Line *ABC* shows the temperature of complete amorphization of the polymer as a function of n-decane amount present in the initial mixture. Line *ABD* corresponds to the temperature boundary of transformation of the two-phase system into a single-phase one, namely, a molecular mixture of LDPE melt and n-decane (segment *AB*) or a solution of n-decane in the amorphous regions of LDPE (segment *BD*).

As a result of extraction, two phases coexist below line *ABD* irrespective of the composition of the mixture: a solution of n-decane in amorphous regions of LDPE and a solution of macromolecules extracted from LDPE in n-decane. The temperature dependence of the composition of the former phase is described by line *BD* and that of the latter one is described by line *EA*. In the case of $w_2 < w_{2B}$, the extraction equilibrium arising upon the stepwise heating of the mixture (see curve *BD*) is transformed into osmotic equilibrium, which is accompanied by complete dissolution of the latter phase in the former one.

It is necessary to emphasize that the phases coexisting below line *ABD* do not possess features inherent in phases according to the classical definition.[3] Indeed, real component exchange, which may give rise to true phase equilibrium in the SC polymer – LMM liquid system, becomes thermodynamically allowed only when all macromolecules of the initial polydisperse polymer acquire translational mobility. This is possible only after the disappearance of all crystallites functioning as cross-links for the polymer networks, *i.e.*, after the temperatures corresponding to line *ABC* have been attained.

In the temperature – concentration field of the phase diagrams of a LDPE mixture with n-decane (see Fig. 5*b*), lines *FGH*, *ABC*, *ABD* and *EA* define four domains:

domain *I* corresponds to a single-phase molecular mixture of n-decane and an LDPE melt;

domain *II* corresponds to a single-phase physical gel: a solution of n-decane in the amorphous regions of LDPE;

domain *III* corresponds to a two-phase system, with one phase being a solution of extracted short-chain LDPE macromolecules in n-decane and the other phase being a solution of n-decane in amorphous regions of LDPE; and

domain *IV* corresponds to a two-phase system, with one phase being a solution of amorphized LDPE in n-decane and the other phase being a solution of n-decane in amorphized LDPE.

Since the SC polymer is a thermodynamically non-equilibrium system below line *ABC*,[1, 2, 168] binary systems containing a solution of the LMM compound in such a polymer are even more non-equilibrium. These states correspond to domains *II* and *III* of the diagram in which a thermomechanical equilibrium is established, which is discussed in detail by Mizerovskii *et al.*[168] Domain *III* is characterized by osmotic equilibrium (defined by line *BD*) as a result of unidirectional diffusion of the LMM component molecules into the amorphous regions of the polymer. Furthermore, extraction equilibrium can be set up in the system if short-chain macromolecules have not been pre-extracted from the polymer sample. All these sorts of equilibrium are not classical phase equilibria; therefore, the Gibbs phase rule, which was formulated for equilibrium systems, cannot be properly applied to the 3D-strained systems existing in the single-phase (*II*) and two-phase (*III*) domains.

Below line *ABC*, only the macromolecules dissolved in the amorphous regions of the SC polymer and not involved in the formation of crystallites migrate to the solvent bulk. The amount of these macromolecules regularly increases during the gradual destruction of crystallites with increasing temperature (see line *EA* in Fig. 5 *b*). Therefore, the thermodynamic characteristics (molecular mass distribution, chemical potential, *etc.*) of the polymer component in the

coexisting phases do not coincide. In particular, the kinematic viscosity (η) of a 1% toluene solution of the initial LDPE sample at 90 °C (η = 0.99 mm^2 s^{-1}) markedly exceeds the kinematic viscosity of the LDPE sample taken from the extraction solution at 70 °C (η = 0.47 mm^2 s^{-1}). This indicates that the average molecular mass of extracted LDPE is significantly lower than that of the initial sample. This observation provides additional evidence for the inapplicability of the phase rule to systems located in domain *III*; it can be applied only to systems in domains *I* and *IV*. Meanwhile, the lever rule is applicable to domains *III* and *IV*.

An example of phase diagram of an SC polymer mixture with a poor solvent (second type) is shown in Fig. 6 for the iso-PP – DBP system.[189]

As applied to this system, the optical method can be used to detect the above-described events **1**, **2**, **3** and **4**, which account for the change in the state of the system during heating. Unlike the SC polymer – good solvent system where event **4**, which reflects mixing of two optically transparent phases, occurs at T_{min}^{am}, in this case, it occurs at a higher temperature. The state of the system at the time points of these events is illustrated by photographs 1 – 6 in Fig. 6.

In the diagram being discussed, lines *BD*, *BC* and *AB* are based on the temperatures of events **1**, **2** and **3**, respectively. The left-hand (*AM*) and right-hand (*NB*) branches of the binodal were constructed using the temperature values of event **4**. The upper critical solution temperature could not be determined because of the thermal destruction of DBP, which is already detected after 2 h of system annealing at 240 °C.

The thermodynamic meaning of line *ABC* is the same as in the case of good solvent. The curve formed by lines *AM*, *NB* and *BD* marks the temperature boundary of conversion of a two-phase system to a single-phase one: a solution of the LMM liquid in an SC polymer is formed from the initial system on line *BD*, while on binodal lines *AM* and *NB*, the system composed of a solution of the LMM component in a

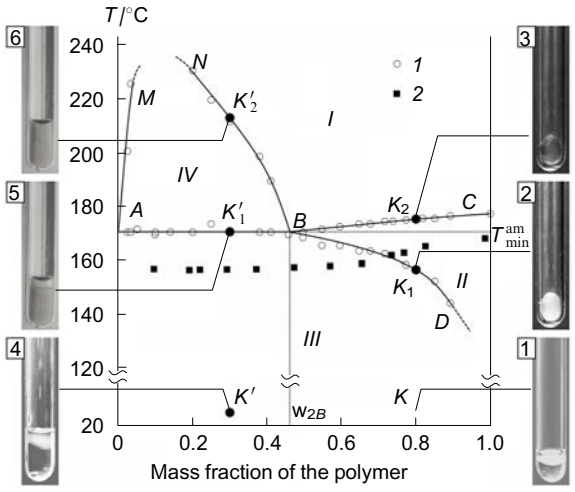


Figure 6. Phase diagram of iso-PP mixtures with DBP[189] supplemented by photographs (1 – 6), which illustrate the state of the mixtures at different points of the temperature – concentration field (for explanations, see the text).
(*1*) Data of the optical method, (*2*) maxima of the endothermic peak from DSC data.

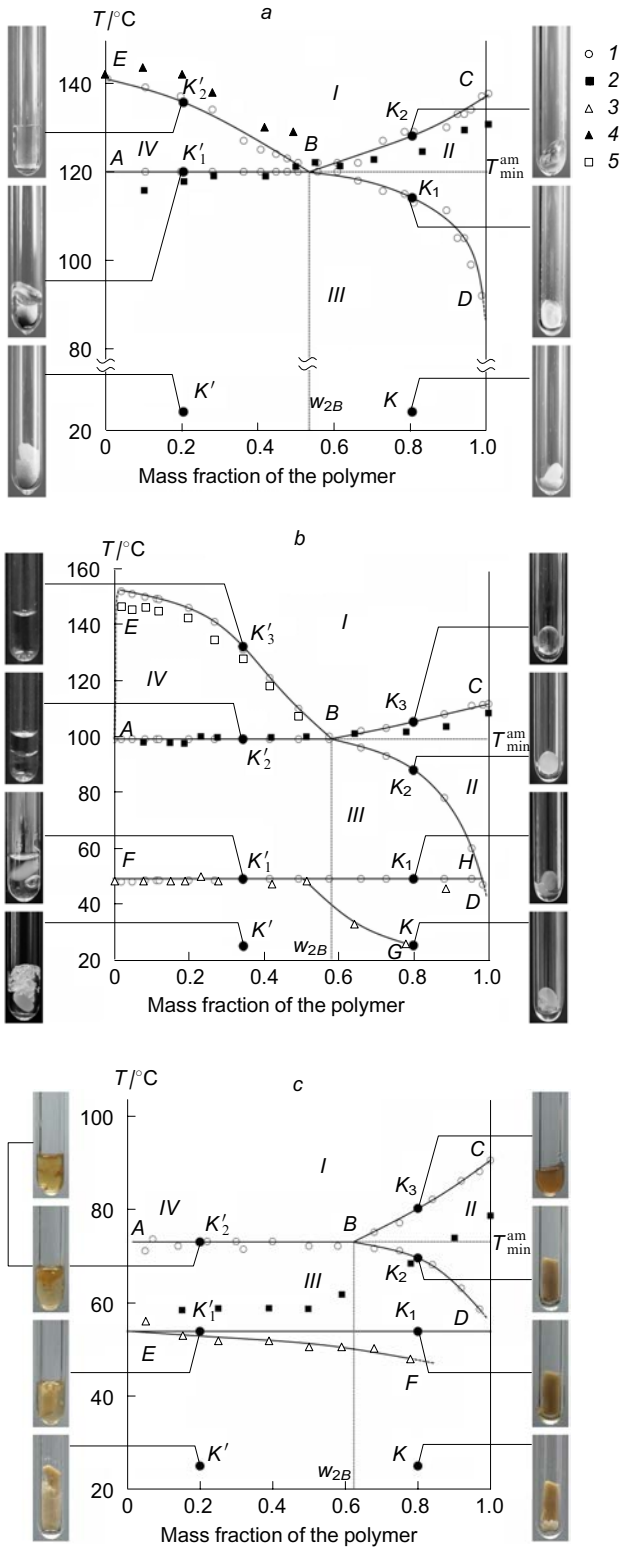


Figure 7. Phase diagrams of mixtures: HDPE with TCB (*a*),[191] LDPE with thymol (*b*)[196] and poly[3,3-bis(azidomethyl)oxetane] (PBAMO) with 2,4-dinitro-2,4-diazapentane (DNAP) (*c*)[195] supplemented by photographs, which illustrate the state of the mixtures at different points of the temperature – concentration field (for explanations, see the text).
(*1*) Data of the optical method, (*2*) maxima of the endothermic peak of polymer amorphization, (*3*) maxima of the low-temperature endothermic peaks, (*4*) maxima of the high-temperature endothermic peaks, (*5*) data of the cloud point method.

polymer melt and a polymer solution in the liquid is transformed into a molecular mixture of a polymer melt and the LMM liquid. These lines, together with the liquid – liquid binodal form four domains in the diagram:

domain *I* corresponds to the existence of a single-phase molecular mixture of an iso-PP melt with DBP;

domain *II* corresponds to the existence of a single-phase physical gel — a solution of DBP in the amorphous regions of iso-PP;

domain *III* corresponds to the existence of a two-phase system, with one phase being pure DBP and the other phase being a DBP solution in iso-PP (the solution composition is specified by curve *BD*); and

domain *IV* corresponds to the existence of a two-phase system, with one phase being a solution of iso-PP in DBP and the other phase being a solution of DBP in an iso-PP melt (the component ratio in the solutions is specified by lines *AM* and *NB*).

In this system, the phase rule is applicable only to regions *I* and *IV*, while the lever rule is applicable to domains *III* and *IV*.

We will consider thermodynamic features of the third type diagrams, which reflect the state of SC polymer mixtures with a crystalline LMM compound. Figure 7 shows three phase diagrams for such mixtures, which were reported by Pochivalov *et al.*,[191, 195, 196] and differ conceptually from one another.

As applied to a mixture of HDPE with TCB (see Fig. 7 *a*), the melting point of which is higher than the polymer melting temperature, two events can be detected during heating for polymer-rich compositions, namely, the disappearance of TCB crystals due to their dissolution in HDPE, which remains opaque (event **1**), and the transformation of the opaque polymer granule into an optically transparent liquid (event **2**).

In the case of compositions rich in the LMM component, the formation of an optically transparent liquid phase, that is, a TCB solution in an HDPE melt, coexisting with TCB crystals (event **3**), and the transformation of this two-phase system into a single-phase optically transparent liquid (event **4**) were observed.

Borderlines *BD*, *BC*, *AB* and *EB* in Fig. 7 *a* were constructed using the temperature values corresponding to events **1**, **2**, **3** and **4**. The photographs shown in this Figure reflect the state of the system with $w_2 = 0.8$ and 0.2 at room temperature and at temperatures corresponding to the borderlines. The phase diagram has two curves — *EBD* and *ABC*. Curve *EBD* shows the temperature of dissolution of TCB crystals in a HDPE melt containing TCB (line *EB*) and in the amorphous HDPE regions (line *BD*) as a function of composition of the initial mixture.

Line *ABC* reflects, as above, the melting temperatures of the last crystallites not connected by tie chains *versus* the TCB amount in the initial mixture.

Since curve *EBD* crosses the whole temperature — concentration field, it can be stated that only TCB solutions in HDPE exist above this curve. In other words, at any component ratio, HDPE is the solvent and TCB is the solute; hence, the diagram presented in Fig. 7 *a* characterizes the SC polymer – non-solvent system. In this case, it is appropriate to use the term 'diluent' in order to emphasize the fact that at any composition of the system, the role of the solvent is performed by the polymer.

Below line *EBD*, the system consists of two phases: TCB crystals coexisting with a TCB solution in HDPE melt (domain *IV*) or with a TCB solution in amorphous regions of solid HDPE (domain *III*). Above this line, a TCB solution in HDPE exists as either a molecular mixture of the components (domain *I*) or a single phase gel with cross-links represented by polymer crystallites (domain *II*), the mass fraction of which (degree of crystallinity) depends on the composition and temperature. In view of the above, line *EBD* can be thermodynamically interpreted in a different way. This curve is the temperature boundary between a two-phase and a single-phase systems: line *BD* marks the transformation of the initial system consisting of solid HDPE and TCB crystals into a solution of TCB in the amorphous regions of HDPE, while line *EB* marks the transformation of the system consisting of TCB crystals and a TCB solution in an HDPE melt into a molecular mixture of HDPE and TCB.

The figurative point *B* marks the lowest temperature of HDPE amorphization in the presence of $(1 - w_{2B})$ of dissolved TCB. In other words, at this point, both HDPE crystallites and TCB crystals disappear and the two-phase system is transformed into a single-phase molecular mixture.

Next we will discuss the dissolution of LMM component crystals in an SC polymer. Pochivalov *et al.*[191, 196] demonstrated that readily sublimable crystalline compounds dissolve by the vapour-phase mechanism. Figure 8 presents the results of experiments on heating HDPE mixtures with TCB without direct contact between the components for compositions with $w_2 = 0.8$ (Fig. 8 *a* – *c*) and 0.2 (Fig. 8 *d* – *f*).

In the former case, all TCB crystals (see Fig. 8 *a*) disappear at point K_1 (see Fig. 7 *a*) in line *BD*; as this takes place, the cylindrical polymer sample increases in size and remains opaque (Fig. 8 *b*). The opacity disappears at point K_2, while the cylindrical sample loses shape, being converted to a liquid (see Fig. 8 *c*). In the mixture containing an excess of the LMM compound, the polymer granule turns into a transparent liquid at point K'_1, with TCB crystals being still present in the tube (see Fig. 8 *e*). At point K'_2, these crystals disappear, while the volume of the

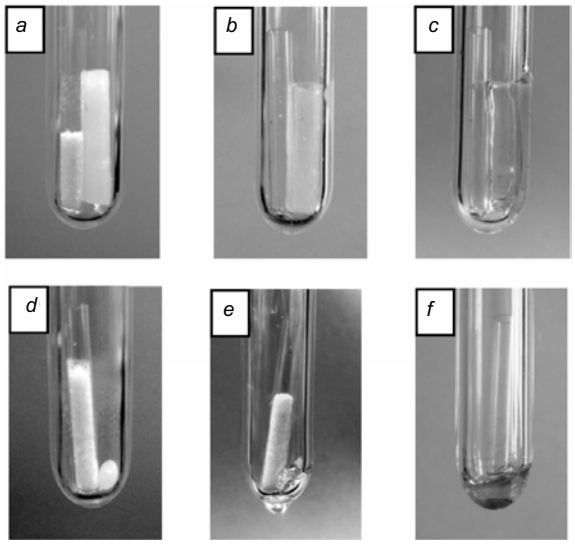


Figure 8. Photographs illustrating the state of the HDPE mixture with TCB in the absence of a direct contact between the components at points K (*a*), K_1 (*b*), K_2 (*c*), K' (*d*), K'_1 (*e*), K'_2 (*f*) in Fig. 7 *a*.

Table 5. Thermodynamic parameters of polyolefin mixtures with TCB.[191]

System	T_m /°C	T_{min}^{am} /°C	β	$1-w_{2B}$
LDPE – TCB	111.6	103.0	0.93	0.29
HDPE – TCB	138.0	120.0	0.86	0.45
Iso-PP – TCB	176.4	136.0	0.77	0.79

polymer melt containing dissolved TCB increases (see Fig. 8 *f*).

Comparison of the positions of the figurative point *B* in the phase diagrams of three mixtures of TCB with polyolefins can also be used to characterize the thermodynamic affinity of their components by the parameter β and the difference $1-w_{2B}$ (Table 5). The highest TCB affinity is inherent in iso-PP, while the lowest affinity is characteristic of LDPE.

Figure 7 *b* shows the phase diagram of an LDPE mixture with thymol, the melting point of which in the pure state is 49.5 °C. In this case, events **1**–**4** described above are preceded by melting of the thymol crystals at 49.5 °C, which can be observed for the $0 < w_2 < 0.98$ composition range. The state of two mixtures (polymer-rich and polymer-lean) at room temperature and at temperatures of the indicated events is illustrated by the photographs.

Borderlines *BD*, *BC*, *AB* and *EB* are constructed using the temperature values corresponding to events **1**, **2**, **3** and **4**, respectively, for mixtures of different compositions. The phase diagram containing these lines is similar to the diagram of the iso-PP – DBP mixture (see Fig. 6) and, hence, corresponds to the second type (SC polymer – poor solvent). The diagram has four domains, the thermodynamic interpretation of which is given above.

The difference between the behaviours of the iso-PP – DBP and LDPE – thymol systems is that in the latter case, the UCST is sifted to thymol-rich compositions to such an extent that even with 0.995 mass fractions of thymol in the mixture, the UCST cannot be detected and the left branch of the binodal virtually coincides with the ordinate axis ($w_2 = 0$). Furthermore, below the melting point, thymol dissolves in the solid polymer by the vapour-phase mechanism.

The phase diagram and the photographs presented in Fig. 7 *c* reflect the phase behaviour of an SC polymer mixture with the PBAMO – DNAP crystalline system, virtually unable to undergo sublimation. This phase diagram is similar to that for an SC polymer mixture with a good solvent (see Fig. 5). A specific feature of the PBAMO – DNAP system is a very low rate of diffusion processes taking place in the system. The construction of this diagram required almost eight months of experiments, while construction of other phase diagrams by the optical method took 2 to 3 months.

The data described above lead to the following conclusions. The new interpretation of the phase equilibrium in mixtures of an SC polymer with a liquid or a crystalline LMM compound is based on the view that SC polymers can be described as single-phase internally strained (metastable) 3D structured liquids with intermolecular cross-links represented by crystallites.

In terms of this approach, augmented phase diagrams for these mixtures were constructed for the first time; the diagrams have an additional borderline (*BD*) reflecting the temperature dependence of solubility of the LMM component in the amorphous regions of the polymer. Below this curve, osmotic equilibrium is established in the system, with the role of osmotic cell being played by the polymer, which acts as the solvent for the LMM component acting as the solute.

In terms of their topology, phase diagrams can be classified into three key types: SC polymer – good solvent, SC polymer – poor solvent and SC polymer – LMM crystalline compound. Diagrams of the first type have a borderline that shows the temperature of disappearance of the last polymer crystallites as a function of mixture composition (*ABC*) and a line that shows the temperature dependence of the LMM component solubility in the amorphous regions of the SC polymer (*BD*). For some mixtures, a liquid – liquid binodal with an LCST located above the mentioned lines can also be identified. The second type diagrams contain, apart from the lines indicated above, a liquid – liquid binodal with a UCST, the right branch of which stems from figurative point *B*. The third type diagrams include, instead of the liquid – liquid binodal, a borderline that depicts the solubility of the crystals of the LMM component in its solution in the polymer melt (line *EB* in Fig. 7 *a*). It is noteworthy that mixtures of an SC polymer with a low-molecular-mass crystalline component that melts at a lower temperature than the polymer may have both the first (see Fig. 7 *c*) and second type (see Fig. 7 *b*) phase diagrams.

The appearance of borderline *BD* in the phase diagrams of all three types markedly changes their thermodynamic meaning. In particular, curves *BD* and *ABC* strictly encompass the domain of existence of single-phase thermoreversible metastable gels with intermolecular cross-links represented by crystallites. This gel is a solution of the LMM component in the amorphous regions of the SC polymer. In the two-phase domain located below line *BD*, this gel coexists with the pure LMM component (in the general case, with a solution of relatively short extracted macromolecular segments in the LMM liquid). The borderlines *ABC* and *BD* are not phase boundaries, according to the classical meaning of this term, and the systems occurring within the domains they encompass do not obey the Gibbs phase rule.

A new thermodynamic interpretation was given for the figurative point present in the phase diagram, which is commonly regarded as a monotectic or eutectic point. It was shown that the position of this point determined experimentally can be used to estimate the degree of thermodynamic affinity of the mixture components.

4. Differential scanning calorimetry in studies of phase equilibrium

Differential scanning calorimetry is widely used to construct phase diagrams (see Table 1) with the following assumptions:

— the polymer melting temperature corresponds to the endothermic peak whether or not this temperature refers to melting of pure polymer or melting in the presence of the LMM component;

— for mixtures of SC polymers with crystalline LMM components with similar melting temperatures, the high-temperature endothermic peak on the left of the eutectic point reflects melting of the LMM component and a set of such temperatures forms the liquidus line;

— extrapolation of the endothermic peak maxima obtained at different heating rates to the zero heating rate gives a true melting temperature of the polymer;

— the most objective information on transformations in a binary mixture can be gained by repeated heating of the mixture in a calorimeter after preliminary homogenization, which provides a sharp increase in the contact surface area between the components; note that mixtures containing slowly crystallizing polymers, such as PBAMO, should be kept at room temperature before the second heating for a period that would be sufficient for completion of structuring in the polymer component.[195]

The DSC curves measured during the second heating of SC polymer – LMM component mixtures of various composition studied by Pochivalov and co-workers [184, 193, 195, 196] are shown in Fig. 9. It can be seen that two endotherms are recorded by the instrument for an LDPE mixture with *p*-xylene (see Fig. 9 *a*, curves *2 – 12*). As the polymer content in the mixture increases in the $0.3 < w_2 < 0.69$ range, the low-temperature endotherm is first broadened and then separates into two peaks. One of these peaks occurs at a constant temperature, which is ~ 4 °C higher than the reference value for the *p*-xylene melting point (11.5 °C), and the other occurs at a lower temperature, which decreases with decreasing content of *p*-xylene in the mixture. The decrease in the *p*-xylene content is also accompanied by decreasing intensity of both peaks, so that only the first peak is observed at $w_2 = 0.80$, while at $w_2 > 0.80$, the heat of melting of *p*-xylene cannot at all be determined by DSC. Simultaneously, the intensity and the temperature of the second (high-temperature) endotherm increase.

Considering the results of optical experiments, the DSC data can be interpreted in the following way.[171] For compositions $w_2 > w_{2B}$ (curves *1 – 9*), they reflect *p*-xylene melting and dissolution in the amorphous LDPE regions and the thermomechanical amorphization of the polymer induced by the combined action of the swelling pressure and temperature. In the $w_2 < w_{2B}$ range (curves *10 – 12*), these endothermic peaks reflect also mixing of the molecular mixture of an LDPE melt containing $(1 - w_2)$ of *p*-xylene, which appears at $T_{\min}^{\text{am}}$, with an excess of *p*-xylene. It can be seen from the DSC curve that the heats of processes that take place after *p*-xylene melting are indistinguishable by calorimetry. Hence, in analysis of DSC curves, melting of an SC polymer in the presence of the LMM component can be considered only conditionally having in mind the integral heat of formation of the molecular mixture of the LDPE melt and *p*-xylene. Therefore, while constructing the phase diagrams from DSC data, we used temperature values corresponding to the onset of deviation of the curves from the baseline (*p*-xylene melting point) and to the maximum of the last endothermic peak (the temperature of complete LDPE amorphization).

These temperatures were put on the phase diagram of an LDPE – *p*-xylene mixture (see Fig. 5 *a*). It can be seen that

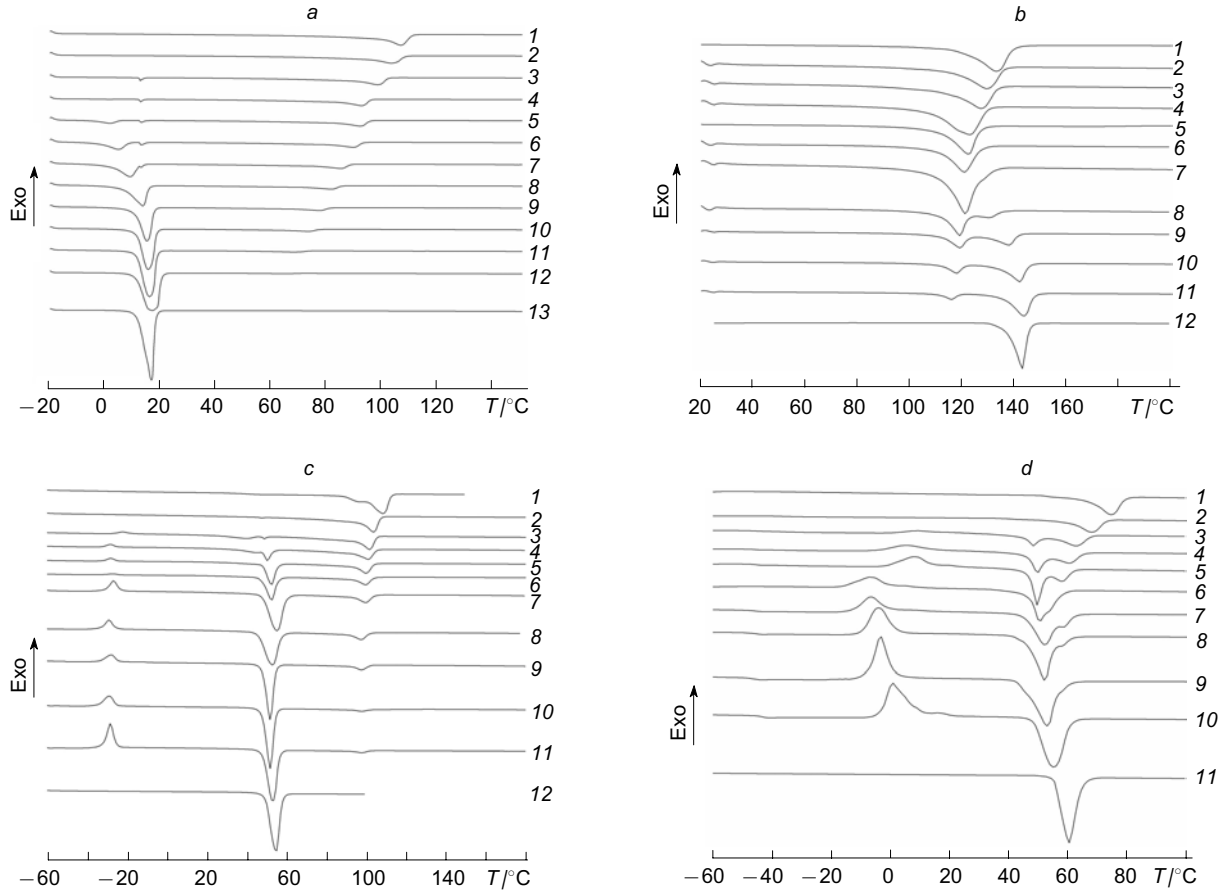


Figure 9. DSC thermograms obtained during the second heating of mixtures: LDPE with *p*-xylene (*a*),[184] HDPE with TCB (*b*),[193] LDPE with thymol (*c*),[196] PBAMO with DNAP (*d*).[195]
(*a*) $w_2 = 1$ (*1*), 0.907 (*2*), 0.799 (*3*), 0.691 (*4*), 0.667 (*5*), 0.603 (*6*), 0.499 (*7*), 0.402 (*8*), 0.301 (*9*), 0.199 (*10*), 0.100 (*11*), 0.027 (*12*), 0 (*13*);
(*b*) $w_2 = 1$ (*1*), 0.937 (*2*), 0.872 (*3*), 0.700 (*4*), 0.611 (*5*), 0.569 (*6*), 0.494 (*7*), 0.416 (*8*), 0.279 (*9*), 0.202 (*10*), 0.0973 (*11*), 0 (*12*);
(*c*) $w_2 = 1$ (*1*), 0.887 (*2*), 0.781 (*3*), 0.643 (*4*), 0.514 (*5*), 0.420 (*6*), 0.277 (*7*), 0.232 (*8*), 0.178 (*9*), 0.150 (*10*), 0.079 (*11*), 0 (*12*);
(*d*) $w_2 = 1$ (*1*), 0.892 (*2*), 0.779 (*3*), 0.682 (*4*), 0.590 (*5*), 0.496 (*6*), 0.391 (*7*), 0.247 (*8*), 0.154 (*9*),0.050 (*10*), 0 (*11*).

temperatures of the second endothermic peak are located below the data obtained by optical method over the whole range of compositions. This means that line *ABC* can be drawn only approximately using DSC data. It is also important that, since the temperature of completion of the dissolution of the LMM component in the SC polymer cannot be estimated using DSC, it is impossible to construct borderline *BD*, without which the diagram gives a wrong idea of the state of the system below line *ABC*. The lines *EFG* and *FH*, which have appeared in the phase diagram, do not change its thermodynamic interpretation, but make it possible to evaluate characteristic features of the phase structure formed in the mixture after homogenization and subsequent cooling.

Below line *EFG*, which corresponds to melting of *p*-xylene, the system still consists of two phases, but one phase (*p*-xylene) has converted from the liquid to crystalline state. The composition of the second phase depends on the possibility of dissolution of crystalline *p*-xylene in LDPE. If the vapour-phase dissolution mechanism is involved, the second phase will be represented by a solution of *p*-xylene in amorphous regions of LDPE, like that above line *EFG*. Otherwise, the second phase will be represented by pure LDPE. Curve *FH*, which describes the endothermic peak with the temperature at maximum of <11.5 °C, is interpreted [184] in terms of classical views stating that the melting temperature of LMM compound crystals decreases with decreasing crystal size.[201] *p*-Xylene crystals with a size smaller than the size of these crystals in their own phase are formed in the pores of the capillary porous body, which arises as the molecular mixture is cooled down and brought from domain *I* to domain *III* (see Fig. 5 *a*). The matrix of a capillary porous body is a physical gel, with crystallites acting as the network cross-links, while the pores are filled by *p*-xylene, which is released upon phase separation and crystallizes during cooling down to -70 °C in the DSC experiment. The structure of the capillary porous body after removal of *p*-xylene *via* extraction into isopropyl alcohol is clearly seen in the optical microscopic image (Fig. 10). As the amount of the polymer in the initial mixture increases, the melting point of *p*-xylene crystals formed in the pores decreases (see Fig. 5 *a*, line *FH*) and, hence, the size of crystals decreases. The calculation by the Gibbs–Thomson equation demonstrated that the characteristic size of these crystals increases from 6 to 17 nm as *p*-xylene mass fraction in the initial mixture with LDPE is increased from 0.2 to 0.6.[184]

Analysis of the melting exotherms of iso-PP and its mixtures with DBP (poor solvent) demonstrated that only one peak is detected in the DSC experiment, reflecting the heat of calorimetrically indistinguishable processes of DBP dissolution in iso-PP and thermomechanical amorphization of the polymer in the presence of dissolved DBP. No heat of mixing of two phases is detected as the system arrives at the liquid–liquid binodal line. The temperature values corresponding to the found peak are shown in Fig. 6, which indicates that they are regularly located below the optical data.[190]

The temperature curves of HDPE, TCB and their mixtures are illustrated in Fig. 9 *b*. When $w_2 = 0.5$, a second endothermic peak appears in the curves, reflecting the heat of dissolution of excess TCB crystals in an HDPE melt already containing dissolved TCB. Comparison of calorimetric and optical data shown in Fig. 7 *a* indicates once again that line *BD* cannot be drawn, in principle, using the DSC data, while line *ABC*, as well as line *EB*, reflecting the solubility of TCB in an HDPE melt, can be drawn only roughly.

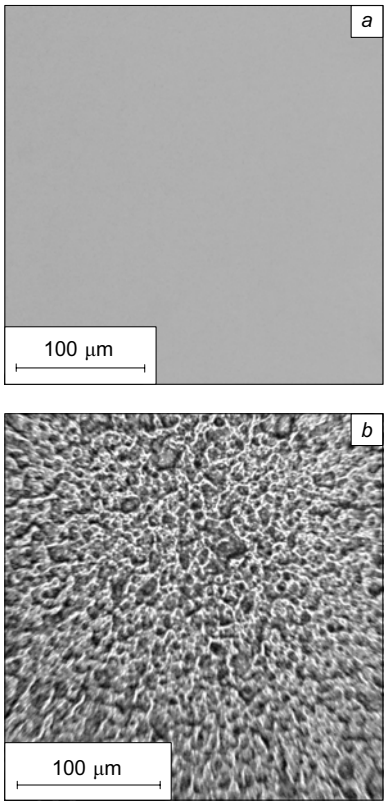


Figure 10. Photomicrographs of phase structure in a PBAMO mixture with a three-component plasticizer ($w_2 = 0.4$) in the homogeneous state at 90 °C (*a*) and at room temperature (*b*).[188]

While comparing data presented in Fig. 4 *a* with the DSC curves being discussed, one can note that, when the temperature scan rate is increased from 8 (Ref. 60) to 10 °C min^{-1} (Ref. 193), the low-temperature peaks for compositions $w_2 > w_{2B}$ (Fig. 7 *a*) are no longer detected.

Attention should be paid to the interpretation proposed by Smith and Pennings [60] for the curve formed by the set of temperatures corresponding to the endothermic peak maxima. In the opinion of the authors, this curve corresponds to melting of the eutectic mixture, that is, it continues the solidus. In our opinion, this line, like line *FH* in the phase diagram of the LDPE mixture with *p*-xylene (see Fig. 5 *a*), reflects the dependence of the melting point of small-sized TCB crystals on the mixture composition. The position of the solubility curve *BD* in the diagram suggests that the isotherm, which was obtained using DSC [60] and reflecting a polymorphic transition of HMB crystals at 111 °C in the phase diagram of its mixture with HDPE, is terminated at the LMM component volume fraction of 0.2, because at a lower content of HMB, it is completely dissolved at this temperature in the amorphous regions of HDPE by the vapour-phase mechanism.

The DSC curves of LDPE, thymol and their mixtures are shown in Fig. 9 *c*. They differ from the DSC curves of LDPE mixtures with *p*-xylene (see Fig. 9 *a*) only by the presence of an exothermic peak at -25 °C, which reflects the heat of additional crystallization during the second heating of thymol that did not have time to crystallize during cooling of the homogenized mixture. The phase diagram shown in Fig. 7 *b* was constructed using the tem-

peratures corresponding to the maxima of the thymol and LDPE melting endotherms, which made it possible to determine positions of lines *FH* and *FG* and (only roughly) curve *ABC*. These lines reflect the melting points of normal- and small-sized thymol crystals dispersed in the polymer matrix upon thermally induced phase separation and the temperature of complete amorphization of LDPE as functions of mixture composition.

The DSC curves shown in Fig. 9 *c* indicate that the heat effects in the LDPE mixture with thymol [196] are completed near the second endothermic peak. This means that for this mixture, like for an iso-PP – DBP mixture,[190] the temperature in the $w_2 < w_{2B}$ domain where the system becomes a single phase cannot be unambiguously determined by DSC. This temperature can be found by cloud point measurement (see Fig. 7 *b*). Since the cloud point method is kinetic, like DSC, the results, as expected, do not coincide with the results of the optical method.

Figure 9 *d* depicts the DSC thermograms of PBAMO, DNAP and their mixtures containing an exothermic peak for additional crystallization of DNAP (curves *3* – *10*) and an endothermic peak of an intricate shape, which reflects a combination of melting of small-sized and normal-sized DNAP crystals in the pores of the capillary porous body, dissolution of liquid DNAP in amorphous regions of PBAMO and polymer amorphization.[195] Due to the similarity of the DNAP melting point and the temperature of PBAMO amorphization in the presence of this plasticizer, which is dissolved in the polymer during the DSC experiment, these processes cannot be separated. Therefore, phase diagrams shown in Fig. 7 *c* were constructed using temperatures [195] corresponding to onset of the first and the maximum of the second endotherms.

The dependences of polymer amorphization temperature on the mixture composition obtained by different methods are substantially different (see Fig. 7 *c*). The considerable discrepancy between the DSC and optical data is due to the fact that long-term stepwise heating is accompanied by restructuring of the crystalline regions of PBAMO, and new, more perfect, rather than the initial crystallites melt at the temperature determined by the optical method. Judging by the position of line *EF* constructed using temperatures of the onset of the first endotherm, the small-sized DNAP crystals are formed on cooling of the homogenized mixture virtually at any composition of the mixture.

The discussion of the phase diagrams can be summarized by stating that amorphization of polyolefins both in the absence and in the presence of an LMM component takes place in a very broad temperature range. The causes for existence of this range are discussed in our publications.[190, 191] In particular, it was shown that the endotherm reflecting the heat of amorphization of the SC polymer describes both the thermomechanical destruction of crystallites connected by tie chains and the purely thermal melting of the last crystallites not connected to one another. The latter of the indicated processes takes place at a definite temperature, while the former one occurs at a lower temperature over the whole range of compositions. It was found for various polyolefins that the temperature of complete amorphization of the SC polymer found by the optical method never coincides with the endotherm maximum in the DSC curve.

In some studies published at the end of the 20th century (*e.g.*, Ref. 202), the liquid – liquid binodal in the phase diagrams of amorphous polymer – LMM compound mixtures was obtained using high-sensitivity DSC instruments. No data of this type are yet available from the literature for mixtures containing an SC polymer.

Thus, DSC should not be used as the main method when studying the phase equilibria in SC polymer – LMM component mixtures; however, DSC can detect processes and structural features unnoticed by other methods, such as polymer glass transition in the presence of the LMM component [72, 73] and glass transition of the LMM compound;[185] melting of LMM crystals formed in the polymer matrix with a smaller size than in the own phase;[195, 196] change in the crystal structure of the LMM component;[60] eutectic behaviour of mixed solvents at low temperature;[188] transformation of the polymer crystal lattice;[157, 158] and existence of groups of crystallites of different degrees of perfection (stress) that melt at different temperature in a polymer sample.[203] In addition, by varying temperature scan rate in the DSC experiment, one can model the conditions of real industrial processes and estimate key process parameters.

The shape of the calorimetric curve on heating the mixture is specified by an integral function that reflects a combination of processes differing in the duration and mechanism (melting, dissolution) and may be accompanied by either heat absorption or heat release. Therefore, it is clear from purely geometric considerations that the temperatures of endotherms and exotherms can only be used for constructing approximate borderlines in the phase diagrams. The curve *ABC* for complete polymer amorphization (see Figs 5 – 7) and the curve *EB* for solubility of the crystalline LMM component in a polymer melt (see Fig. 7 *a*) can serve as examples. For the same reason, it is not for sure that extapolation of DSC data to the zero heating rate would increase the efficacy of this method for the construction of equilibrium phase diagrams.

Without a way to distinguish between the temperature of completion of dissolution of the LMM component in the SC polymer and the temperature of completion of mixing of two liquid phases, it is impossible to draw line *BD* (see Figs 5 – 7) or the liquid – liquid binodal line using DSC.

The advantage of DSC is that it enables fast construction of dynamic (engineering) phase diagrams, which can be used for estimating the conditions for fabrication of functional polymeric materials (membranes, granules, powders, *etc.*) and features of the phase structure arising when single-phase binary mixtures are transferred to domain *III* (see Figs 5 – 7).

5. Phase structure of mixtures of semicrystalline polymers with low-molecular-mass compounds

Proceeding from the new thermodynamic interpretation of phase diagrams, we will consider how the phase structure of mixtures of all three types changes as the mixtures are cooled down from domain *I* to domain *III*. First, we will separately discuss the behaviour of these mixtures for compositions $w_2 < w_{2B}$ and $w_2 > w_{2B}$.

Cooling of a homogeneous mixture comprising an SC polymer and a good solvent (LDPE – *p*-xylene) at $w_2 < w_{2B}$ (see Fig. 5 *a*) is accompanied by crystallization of the polymer in the sample microvolumes arising due to concentration fluctuations. Simultaneously, pure *p*-xylene (in the general case, containing short amorphous macromolecules) is evolved as a separate phase, while the mass fraction of LDPE in the remaining heterogeneous mixture reaches w_{2B}. As the temperature is further decreased, the volume of

p-xylene phase increases, the volume of the crystallizing phase decreases, and the mass fraction of crystallites in this phase increases. The *p*-xylene concentration in its solution in amorphous regions of LDPE is specified by line *BD*.

The morphology of the arising two-phase system depends on the ratio between the composition of the initial mixture w_2 and some critical composition w_c corresponding to transition from the polymer solution in the LMM liquid to the solution of this liquid in the polymer. If $w_2 < w_c$, a suspension of sphere-like polymer particles in the LMM component is formed; if $w_2 \approx w_c$, an interpenetrating structure is obtained; and if $w_2 > w_c$, a dispersion of the LMM component in the polymer, that is, a capillary porous body, which can be considered as a precursor of a polymer membrane, is generated. Pressure produced by the growing drops of the LMM liquid, formed upon phase separation, on the solid matrix surrounding the drops, the decrease in the matrix volume (bulk compressive strain) and crystallization of the polymer give rise to defects, which reduce the mechanical strength of the matrix.

As an example, Fig. 10 shows the photomicrographs of a mixture of PBAMO with a ternary mixture of dinitrodiazaalkanes, which is a good solvent ($w_2 = 0.4$).[188] Cooling of the pre-homogenized mixture (Fig. 10 *a*) to room temperature is accompanied by phase separation, giving rise to a dispersion of the plasticizer in a polymer matrix (Fig. 10 *b*).

The morphology of a capillary porous body formed at $w_2 > w_c$ is illustrated by Fig. 11. It can be seen that, after removal of the LMM component, the thermally induced phase separation of the mixture gives interconnected large ($\sim$10 m) sphere-like particles with small pores. Analysis of phase diagrams (see Fig. 5 *a*) demonstrated that the total volume of the evolved liquid and the average size of liquid drops decrease with increasing amount of the polymer in the mixture.

When a mixture of iso-PP with DBP is transferred from domain *I* to domain *IV* (see Fig. 6), the initially homogeneous system is separated into two liquid phases, which form an internally unstrained emulsion. The temperature dependence of the compositions of coexisting phases is described by the left- and right-hand branches of the binodal. The emulsion structure depends on the relationship between the composition of the initial mixture w_2 and the composition corresponding to the upper critical solution temperature (w_{2UCST}). If $w_2 < w_{2UCST}$, a dispersion of polymer-rich liquid phase drops in a polymer-lean liquid phase is formed; if $w_2 \approx w_{2UCST}$, an interpenetrating phase structure is formed; and if $w_2 > w_{2UCST}$, the polymer-lean liquid phase is dispersed in the polymer-rich liquid phase. In

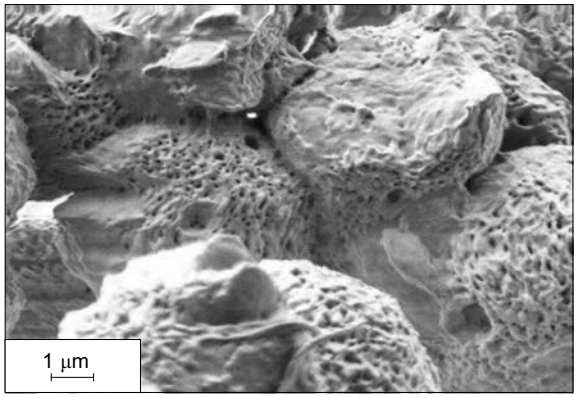


Figure 11. Electron microscopy image of the capillary porous body formed from an LDPE mixture with *p*-xylene at $w_2 = 0.3$.

the last-mentioned case, further cooling of the system does not change the number of phases or the already formed morphology, but is accompanied by crystallization of the polymer. As a result, the polymer-rich matrix phase is converted to a gel with network cross-links represented by crystallites (a solution of the LMM liquid in the SC polymer), whereas the dispersed phase rich in the LMM component is converted to a low-concentration suspension of sphere-like particles of the same gel in the LMM liquid. Polymer crystallization and separation of the LMM component during further cooling bring this two-phase system into a 3D strained state, with the degree of strain determining the defectiveness of the resulting capillary porous bodies. Since the primary formation of the dispersion does not induce mechanical strain, presumably, SC polymer mixtures with poor solvent would give much less defective capillary porous bodies than the mixtures with good solvents considered above.

The photomicrographs shown in Fig. 12 illustrate the phase structure evolution during cooling of an iso-PP – DBP mixture ($w_2 = 0.38$). It can be seen that the mixture that is homogeneous in domain *I* (Fig. 12 *a*) undergoes phase separation on going to domain *IV* and forms a dispersion of the polymer-lean phase in the polymer-rich phase (Fig. 12 *b*). On further cooling of the mixture down to domain *III*, the polymer crystallizes, which is accompanied by a sharp increase in the opacity (Fig. 12 *c*).

Electron microscopic images of the capillary porous bodies resulting from removal of DBP are shown in Fig. 13. A cellular structure (polymer matrix with nearly

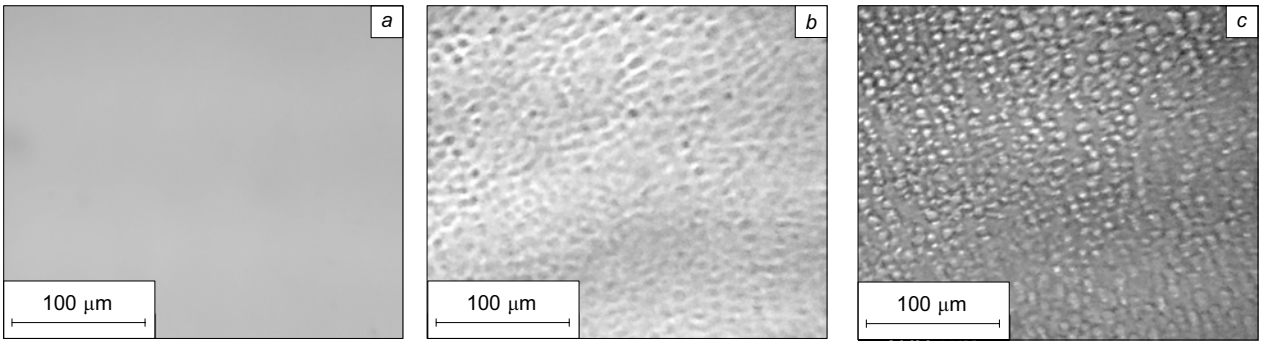


Figure 12. Photomicrographs of the phase structure of an iso-PP – DBP mixture ($w_2 = 0.38$) in domains *I* (*a*), *IV* (*b*) and *III* (*c*) of the phase diagram shown in Fig. 6.

spherical pores) is generated in an SC polymer – poor solvent mixture, which differs substantially from the structure formed in an SC polymer – good solvent mixture (see Fig. 11). The total volume of the pore space and the characteristic pore size of the capillary porous bodies presented in Fig. 13 decrease with increasing amount of the polymer in the initial mixture.

Cooling of a homogeneous mixture of HDPE with TCB, the melting point of which exceeds $T_{\min}^{\mathrm{am}}$, induces the following changes. As curve *EB* in the phase diagram is crossed (see Fig. 7 *a*), TCB crystallizes from its liquid solution in molten HDPE. As the temperature is lowered, the mass fraction of TCB crystals increases, while that of the solution decreases (domain *IV*), with the component ratio in the solution being specified by line *EB*. Crossing line *AB* induces crystallization of the polymer component, the matrix phase being converted to a physical gel, with HDPE crystallites acting as the cross-links and amorphous regions containing dissolved TCB. On further cooling, phase separation continues; however, the growth of the separated TCB crystals is limited to the network of polymer crystallites, which deteriorates the strength characteristics of the system.

As an illustration, Fig. 14 shows photomicrographs of an iso-PP – TCB mixture with $w_2 = 0.2$ during its slow cooling from the homogeneous state at 150 °C (see Fig. 14 *a*). At 133 °C, large (5 – 20 m) needle-like TCB crystals are formed as a dispersion in a mixture of liquid TCB and molten iso-PP (see Fig. 14 *b*). Further decease in the temperature to 117 °C induces crystallization of the polymer in the matrix phase and matrix solidification (see Fig. 14 *c*). At 115 °C, small non-needle TCB crystals appear within the solid matrix bulk (see Fig. 14 *d*). As room temperature is attained, the amount of small crystals increases (see Fig. 14 *e*), while the polymer matrix in which both large and small crystals are dispersed virtually does not contain dissolved TCB any longer.

The structure of the capillary porous body obtained from an HDPE – TCB mixture with $w_2 = 0.34$ after removal

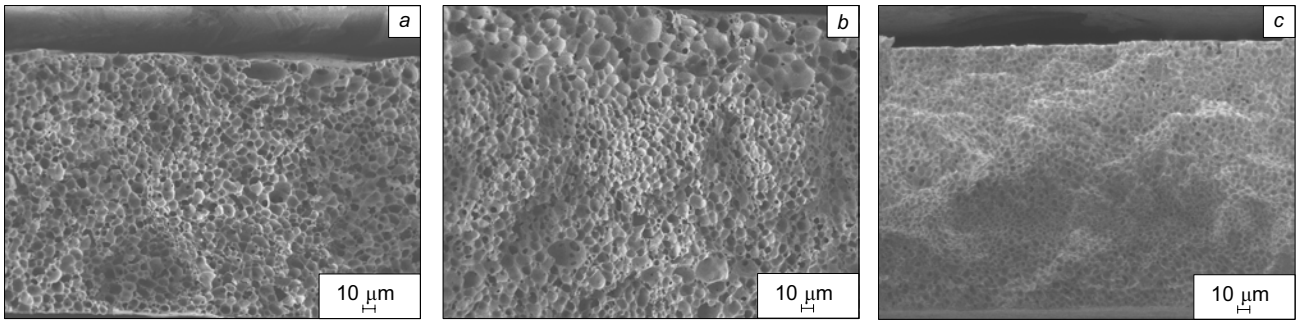


Figure 13. Electron microscopy images of the capillary porous bodies formed from iso-PP mixtures with DBP studied in Ref. 189. $w_2 = 0.2$ (*a*), 0.25 (*b*) and 0.3 (*c*).

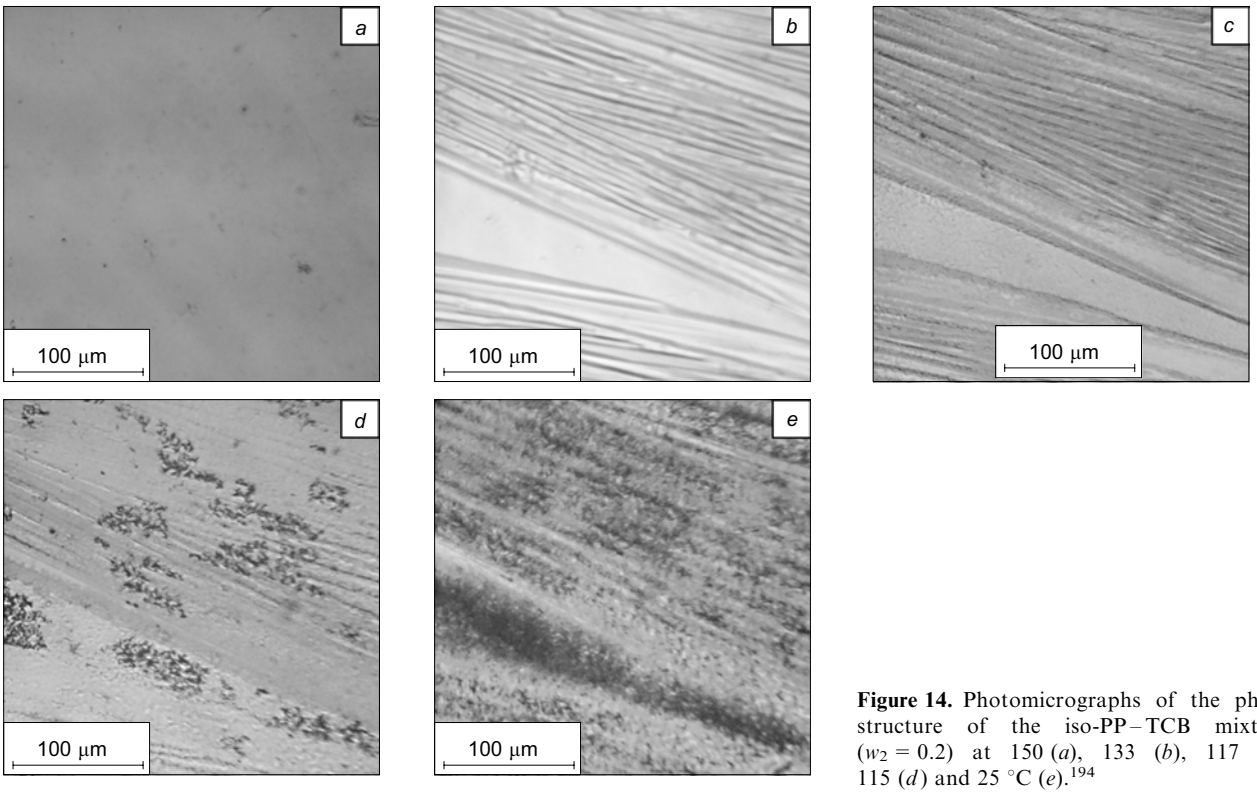


Figure 14. Photomicrographs of the phase structure of the iso-PP – TCB mixture ($w_2 = 0.2$) at 150 (*a*), 133 (*b*), 117 (*c*), 115 (*d*) and 25 °C (*e*).[194]

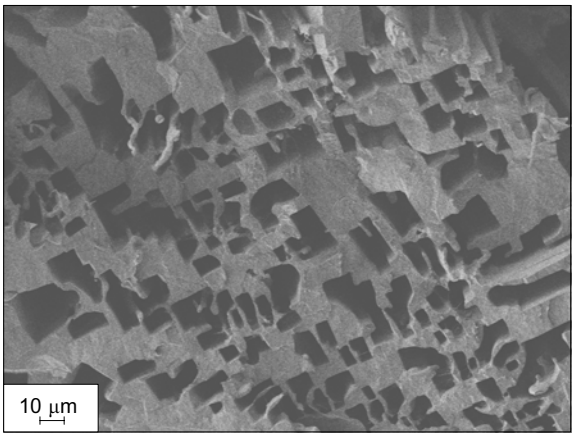


Figure 15. Electron microscopy image of the capillary porous body formed from an HDPE mixture with TCB studied in Ref. 191. $w_2 = 0.34$.

of the LMM component by evacuation at 60 °C for 1 h is demonstrated in Fig. 15. In this case, pore morphology repeats the shape of TCB crystals formed on cooling.

The cooling-induced structuring of SC polymer mixtures with crystalline LMM compounds that melt below $T_{\min}^{am}$ but above room temperature (LDPE – thymol [196] and PBAMO – DNAP [195] systems) does not differ fundamentally from the structuring of the above-considered mixtures of SC polymers with poor and good solvents. Depending on the composition of the mixture, one of the three above-described morphologies is formed: dispersion of the polymer-rich phase in the polymer-lean phase; interpenetrating structure; and dispersion of the polymer-lean phase in the polymer-rich phase. A specific feature of these mixtures is that, at room temperature, the LMM component is crystallized irrespective of morphology.

Cooling of any of the above homogeneous mixtures with $w_2 > w_{2B}$ below curve *BC* (see Figs 5 – 7) induces crystallization of the polymer giving rise to a single-phase physical gel in which crystallites act as cross-links for the intermolecular bond network. The mass fraction of these cross-links, characterizing the degree of crystallinity for a mixture of a definite composition, increases with decreasing temperature. Transfer of the system below curve *BD* induces phase separation; as a result, the polymer-lean phase becomes dispersed in the polymer-rich phase (gel).

The evolution of the phase structure of an iso-PP – TCB mixture with $w_2 = 0.8$ during cooling from the homogeneous state at 180 °C is reflected in Fig. 16. Of interest is the isothermal structuring kinetics at 130 °C. In some regions, iso-PP crystallizes as a mixture with TCB (see Fig. 16 *b*). Subsequently, these regions increase (see Fig. 16 *b*′, 16 *b*″) and coalesce (see Fig. 16 *b*‴). Finally, a single-phase gel of the same composition as the initial mixture is formed. On further cooling of the system down to 100 °C, TCB crystals of a moderate size appear in the gel (see Fig. 16 *c*) and on cooling down to room temperature, the amount of these crystals increases (see Fig. 16 *d*). The shape of TCB crystals is illustrated by the photomicrograph shown in Fig. 16 *d*′.[194]

While being evolved as a dispersed phase, the low-molecular-mass component occurs in either the liquid (*p*-xylene, DBP and so on) or crystalline (TCB, DNAP) state, depending on its chemical nature. Meanwhile, the matrix phase in domain *III* of the phase diagram always possesses a rigid framework of polymer crystallites connected by tie chains and is subjected to three-dimensional strain.

In this Section, we demonstrate how the new interpretation of phase equilibria in the SC polymer – LMM compound mixtures can be used to predict the change in the morphology of these systems as they are cooled from a homogeneous state. Qualitative analysis based on phase diagrams was illustrated by the results of optical and scanning electron microscopy. Depending on the mixture composition and type of the diagram, phase separation affords a dispersion or a structure of interpenetrating

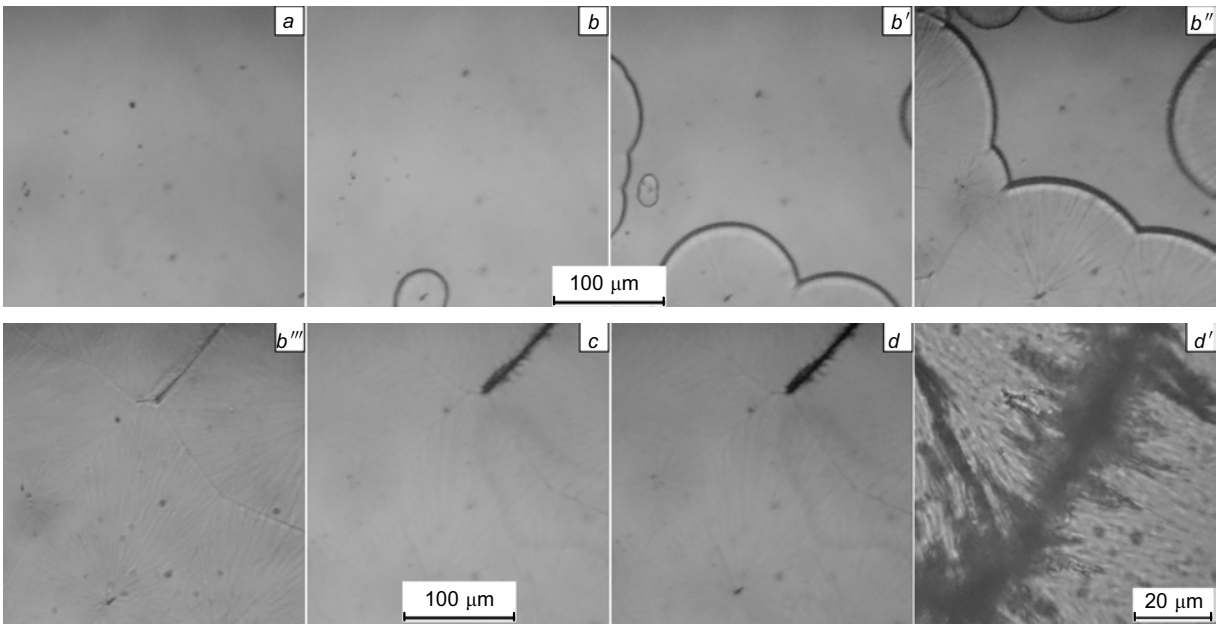


Figure 16. Photomicrographs of the phase structure of the iso-PP – TCB mixture with $w_2 = 0.8$ at 180 (*a*), 130 (*b*), 100 (*c*) and 25 °C (*d*). The series of photomicrographs *b* – *b*‴ describe2 structuring at a constant temperature (130 °C).[194]

phases. A detailed classification of the arising morphologies is necessary in order to develop manufacturing processes for polymeric membranes by thermally induced phase separation and to study the effect of process parameters on their performance.

6. Conclusion

This review gives a systematic account of experimental data on the problem of phase equilibrium in mixtures of SC polymers with liquid and crystalline LMM compounds, which was not addressed in detail previously in Russian or foreign literature. This is a fundamental problem for materials science of polymers, because analysis of phase diagrams helps to develop formulations for the production of new materials, find out how the phase structure of mixtures changes over the operating temperature range, formulate the views on the operating parameters of new processes for manufacturing functional materials (membranes, fibres, granules) and so on.

The review considers two standpoints differing in the interpretation of the phase state of semicrystalline polymers. According to one of them, a crystalline phase state is postulated, *i.e.*, the SC polymer is considered as a single-phase system: a set of defective crystals containing amorphous regions. It is considered that phase equilibrium obeys the Gibbs phase rule and phase diagrams contain the following:

— for an SC polymer mixture with a good solvent, a liquidus line for the polymer component;

— for an SC polymer mixture with a poor solvent, a liquid–liquid binodal line located above the liquidus line;

— for an SC polymer mixture with a crystalline LMM compound, liquidus lines for the low- and high-molecular-mass components and the solidus line.

The positions of these lines in experimental phase diagrams always depend on the temperature scan rate and also on the polymer nature, molecular mass and thermal prehistory, the structure and molecular mass of the LMM compound and so on.

According to the second standpoint, the SC polymer is a single-phase 3D-structured liquid — a physical gel in which the network is formed by crystallites connected by tie chains. According to this approach, one more borderline, reflecting the temperature dependence of solubility of the LMM component in the amorphous regions of the SC polymer, appears in all phase diagrams. This curve can also be interpreted as the temperature boundary for transformation of the two-phase SC polymer – LMM component system into a single-phase solution of the LMM component in the SC polymer on heating. This line indicates that an osmotic equilibrium is present in the system. The solubility curve was constructed in the phase diagrams of more than twenty systems consisting of an SC polymer and a liquid or crystalline LMM component. Together with the curve for complete amorphization of the SC polymer in the presence of an LMM component, this line encompasses the domain of existence of the single-phase physical gel, which cannot be located proceeding from traditional views. The indicated borderlines are not phase boundaries according to the classical meaning of this term and, hence, the phase rule is inapplicable in the diagram domains below these lines.

By analysis and comparison of experimental data, it was possible to identify three main types of phase diagrams, which are schematically shown in Fig. 17. Phase diagrams of the first type (see Fig. 17 *a*) are characteristic of SC polymer mixtures with a good solvent, which can be in either liquid or crystalline state at room temperature. Second type phase diagrams (see Fig. 17 *b*) are characteristic of SC polymer mixtures with a poor solvent, which can also exist in either of the physical states at room temperature. Mixtures of an SC polymer with a crystalline LMM compound, the melting point of which is close to that of the polymer, are characterized by phase diagrams of the third type (see Fig. 17 *c*).

The experimental phase diagrams containing the solubility curve of the LMM component in the SC polymer made it possible to formulate, for the first time, physically clear views on the phase structure evolution of binary mixtures during cooling and on the mechanism of formation of the capillary porous bodies — precursors of polymer membranes. These views were confirmed in DSC and optical and scanning electron microscopy experiments.

The potential of DSC method for the construction of phase diagrams for SC polymer – LMM component mixtures was evaluated. This method is applicable for approx-

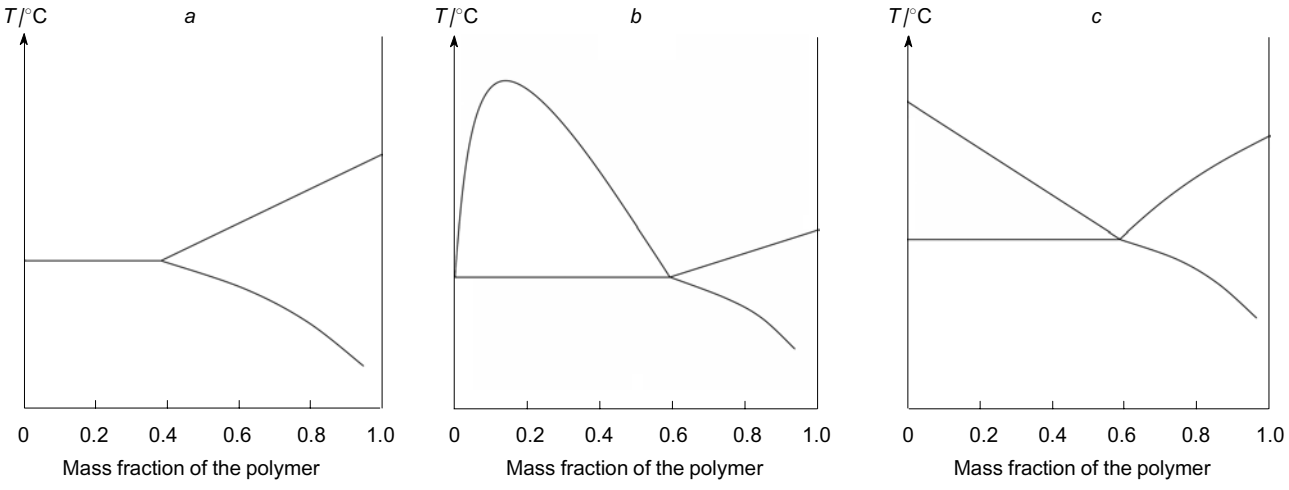


Figure 17. Schematic view of the phase diagrams of SC polymer mixtures with the LMM component, which is either good (*a*) or poor (*b*) solvent for the polymer or is able to crystallize in the same temperature range as the polymer (*c*). The diagrams were constructed within the context of the new interpretation of the phase equilibrium.

imate construction of the curves reflecting the dependence of the temperature of complete amorphization of the polymer on the amount of the LMM component in the mixture and the temperature dependence of the solubility of LMM compound crystals in the SC polymer melt. The solubility curve described above, without which the diagram is incomplete, cannot be constructed, in principle, using DSC. Meanwhile, DSC allows one to determine the polymer glass transition temperature in the presence of the LMM component, detect the formation of LMM component crystals in the polymer matrix that are smaller than the crystals in the own phase of this compound, determine the melting points of these crystals, follow changes in the type of the polymer crystal lattice upon temperature variation and so on.

In view of the foregoing, the following lines of research appear to be most promising for the future:

— development of new theoretical views and construction of equations of state able to satisfactorily describe the phase equilibria in mixtures of SC polymers with LMM compounds;

— study of the phase states of ternary mixtures (SC polymer, solvent and non-solvent);

— evaluation of the possibility of formation of clathrates, intercalates and crystal solvates and their influence on the topology of phase diagrams of binary and ternary mixtures;

— development of a detailed classification of the morphologies resulting from thermally induced phase separation.

The illustrations presented in the review were taken from different sources (the references are given in the figure captions) and modified. Figures 8, 11 – 13, 15, 17 were composed by the authors.

This review was prepared within the State Assignment of the G.A.Krestov Institute of Solution Chemistry, Russian Academy of Sciences (No. 01201260483) and the A.V.Topchiev Institute of Petrochemical Synthesis, Russian Academy of Sciences (theme AAAA-A19-119020490054-7).

The authors are grateful to Corresponding Member of the RAS O.I.Koifman for valuable advice and remarks in the preparation of the review for publication.

References

1. A.E.Chalykh, V.K.Gerasimov. *Russ. Chem. Rev.*, **73**, 63 (2004)
2. G.-M.Guenet. *Thermochim. Acta*, **284**, 67 (1996)
3. J.W.Gibbs. *The Collected Works of J. Willard Gibbs. Thermodynamics*. (New Haven: Yale University Press, 1948). Vol. 1
4. F.A.H.Schreinemakers, H.W.B.Roozeboom. *Die Heterogenen Gleichgewichte von Standpunkte der Phasenlehre*. (Braunschweig: Vieweg, 1913). Vol. III, Pt. 2
5. J.D.van der Waals, Ph.Kohnstamm. *Lehrbuch der Thermodynamik*. Vol. II. (Leipzig: Barth, 1912)
6. P.J.Flory. *J. Chem. Phys.*, **9**, 660 (1941)
7. P.J.Flory. *J. Chem. Phys.*, **10**, 51 (1942)
8. P.J.Flory. *Principles of Polymer Chemistry*. (Chicago, IL: Cornell University Press, 1953)
9. M.L.Huggins. *Ann. N.Y. Acad. Sci.*, **43**, 1 (1942)
10. M.L.Huggins. *J. Phys. Chem.*, **46**, 151 (1942)
11. M.L.Huggins. *Physical Chemistry of High Polymers*. (New York: Wiley, 1958)
12. P.J.Flory. *J. Chem. Phys.*, **13**, 453 (1945)
13. P.J.Flory. *J. Chem. Phys.*, **17**, 1347 (1949)
14. B.H.Zimm, W.H.Stockmayer. *J. Chem. Phys.*, **17**, 1301 (1949)
15. B.H.Zimm, W.H.Stockmayer, M.Fixman. *J. Chem. Phys.*, **21**, 1716 (1953)
16. I.Prigogine. *The Molecular Theory of Solutions*. (New York: Interscience, 1959)
17. D.Patterson, G.Delmas. *Discuss. Faraday Soc.*, **49**, 98 (1970)
18. D.Patterson. *Pure Appl. Chem.*, **31**, 133 (1972)
19. D.Patterson. *J. Polym. Sci., C*, **16**, 3379 (1968)
20. A.Fredenslund, R.L.Jones, J.M.Prausnitz. *AlChE J.*, **21**, 1068 (1975)
21. T.Oishi, J.M.Prausnitz. *Ind. Eng. Chem. Proc. Des. Dev.*, **17**, 333 (1978)
22. U.Weidlich, J.Gmehling. *Ind. Eng. Chem. Res.*, **26**, 1372 (1987)
23. B.L.Larsen, P.Rasmussen, A.Fredenslund. *Eng. Chem. Res.*, **26**, 2274 (1987)
24. P.J.Flory, R.A.Orwoll, A.Vrij. *J. Am. Chem. Soc.*, **86**, 3507 (1964)
25. P.J.Flory. *J. Am. Chem. Soc.*, **87**, 1833 (1965)
26. A.Abe, P.J.Flory. *J. Am. Chem. Soc.*, **87**, 1838 (1965)
27. B.E.Eichinger, P.J.Flory. *Trans. Faraday Soc.*, **64**, 2035 (1968)
28. J.A.R.Renucio, J.M.Prausnitz. *Macromolecules*, **9**, 898 (1976)
29. V.Brandani. *Macromolecules*, **11**, 1293 (1978)
30. V.Brandani. *Macromolecules*, **12**, 883 (1979)
31. K.Sugamiya. *Macromol. Chem.*, **178**, 565 (1977)
32. M.L.Huggins. *Polymer*, **12**, 389 (1971)
33. M.L.Huggins. *Macromolecules*, **4**, 274 (1971)
34. I.Sanchez, R.H.Lacombe. *Macromolecules*, **11**, 1145 (1978)
35. C.Qian, S.J.Mumby, B.E.Eichinger. *J. Polym. Sci., Part B: Polym. Phys.*, **29**, 635 (1991)
36. C.Qian, S.J.Mumby, B.E.Eichinger. *Macromolecules*, **24**, 1655 (1991)
37. C.-C.Chen. *Fluid Phase Equil.*, **83**, 301 (1993)
38. A.Vetere. *Fluid Phase Equil.*, **97**, 43 (1994)
39. N.Orbey, S.I.Sandler. *AIChE J.*, **40**, 1203 (1994)
40. J.Holten-Andersen, P.Rasmussen, A.Fredenslund. *Ind. Eng. Chem. Res.*, **26**, 1382 (1987)
41. F.Chen, A.Fredenslund, P.Rasmussen. *Ind. Eng. Chem. Res.*, **29**, 875 (1990)
42. A.R.Matkar, T.Kyu. *J. Phys. Chem.*, **110**, 16059 (2006)
43. P.Rathi, T.M.Huang, P.Dayal, T.Kyu. *J. Phys. Chem.*, **112**, 6460 (2008)
44. S.Malik, C.Rochas, J.-M.Guenet. *Macromolecules*, **38**, 4888 (2005)
45. M.Anthamatten. *J. Polym. Sci., Part B: Polym. Phys.*, **45**, 3285 (2007)
46. A.E.Nesterov, Yu.S.Lipatov. *Termodinamika Rastvorov i Smesei Polimerov* (Thermodynamics of Polymer Solutions and Blends). (Kiev: Naukova Dumka, 1981)
47. I.M.Balashova, L.V.Mokrushina, A.G.Morachevskii. *Teor. Osnov. Khim. Tekhnol.*, **30**, 366 (1996)
48. H.Matsuyama, T.Maki, M.Teramoto, K.Asano. *J. Membr. Sci.*, **204**, 323 (2002)
49. A.Ferreira, J.Silva, V.Sencadas, J.L.G.Ribelles, S.Lenacroz-Mendez. *Macromol. Mater. Eng.*, **295**, 523 (2010)
50. N.Tang, Q.Jia, H.Zhang, J.Li, S.Cao. *Desalination*, **256**, 27 (2010)
51. H.Tompa. *Polymer Solutions*. (London: Butterworth, 1956)
52. S.P.Papko. *Fiziko-Khimicheskie Osnovy Pererabotki Polimerov*. (Physicochemical Principles of Polymer Processing). (Moscow: Khimiya, 1971)
53. V.I.Klenin. *Termodinamika Sistem s Gibkotsepnymi Polimerami* (Thermodynamics of System Containing Flexible-Chain Polymers). (Saratov: Saratov State University, 1995)
54. S.A.Vshivkov. *Fazovye Perekhody Polimernykh Sistem vo Vneshnikh Polyakh* (Phase Transitions of Polymer Systems in External Fields). (Ekaterinburg: AMB, 2011)
55. S.P.Papkov, V.A.Kargin, Z.A.Rogovin. *Zh. Fiz. Khim.*, **10**, 607 (1937)
56. P.J.Flory. *J. Am. Chem. Soc.*, **63**, 3083 (1941)
57. R.B.Richards. *Trans. Faraday Soc.*, **42**, 10 (1946)
58. S.P.Papkov. *Ravnovesie Faz v Sisteme Polimer – Rastvoritel'*. (Phase Equilibria in Polymer – Polymer Systems). (Moscow: Khimiya, 1981)
59. X.Tan, D.Rodrigue. *Polymers*, **11**, 1310 (2019)

60. P.Smith, A.J.Pennings. *Polymer*, **15**, 413 (1974)
61. E.M.Cernia, C.Mancini, A.Saini. *Kobunshi Kagaku*, **24**, 738 (1967)
62. Y.Kodama, F.L.Swinton. *Brit. Polym. J.*, **10**, 191 (1978)
63. A.Nakajima, H.Fujiwara, F.Hamada. *J. Polym. Sci., Polym. Chem. Ed.*, **4**, 507 (1966)
64. H. Sun, K. B. Rhee, T. Kitano, S. I. Man. *J. Appl. Polym. Sci.*, **73**, 2135 (1999)
65. D.R.Lloyd, K.E.Kinzer,H.S.Tseng. *J. Membr Sci.*, **52**, 239 (1990)
66. S.Liu, C.Zhou, W.Yu. *J. Membr. Sci.*, **379**, 268 (2011)
67. L.Sheng, Y.Du, H.Zhang, Z.Chen, J.Pan, T.Wang, X.Huang, J.He. *Polym. Bull.*, 1 (2019); DOI https://doi.org/10.1007/s00289-019-02733-y
68. S.A.Vshivkov. *Polym. Sci. USSR*, **33**, 522 (1991)
69. M.U.Akhtar, W.W.Focke. *Thermochim. Acta*, **613**, 61 (2015)
70. H.K.Lee, S.C.Kim, K.Levon. *J. Appl. Polym. Sci.*, **70**, 849 (1998)
71. Y.H.Tang, Y.D.He, X.L.Wang. *J. Membr. Sci.*, **409**, 164 (2012)
72. S.Berghmans, H.Berghmans, H.Meijer, J.Mewis. *Polymer*, **36**, 3085 (1995)
73. S.Berghmans, H.Berghmans, H.Meijer. *J. Membr. Sci.*, **116**, 171 (1996)
74. Z.Y.Cui, Ch.H.Du, Y.Y.Xu, G.L.Ji, B.K.Zhu. *J. Appl. Polym. Sci.*, **108**, 272 (2008)
75. J.Yang, D.W.Li, Y.K.Lin, X.L.Wang, F.Tian, Z.Wang. *J. Appl. Polym. Sci.*, **110**, 341 (2008)
76. Zh.Cui, N.T.Hassankiadeh, S.Y.Lee, J.M.Lee, K.T.Woo, A.Sanguineti, V.Arcella, Y.M.Lee. *J. Membr. Sci.*, **444**, 223 (2013)
77. Y.Su, C.Chen, Y.Li, J.Li. *J. Macromol. Sci., Part A*, **44**, 99 (2007)
78. X.Li, X.Lu. *J. Appl. Polym. Sci.*, **101**, 2944 (2006)
79. S.Rajabzadeh, C.Liang, Y.Ohmukai, T.Maruyama, H.Matsuyama. *J. Membr. Sci.*, **423**, 189 (2012)
80. J.T.Jung, J.F.Kim, H.H.Wang, E.Nicolo, E.Drioli, Y.M.Lee. *J. Membr. Sci.*, **514**, 250 (2016)
81. J.T.Jung, H.H.Wang, J.F.Kim, J.Lee, J.S.Kim, E.Drioli, Y.M.Lee. *J. Membr. Sci.*, **559**, 117 (2018)
82. J.Pan, Ch.Xiao, Q.Huang, Ch.Wang, H.Liu. *RSC Adv.*, **5**, 45249 (2015)
83. C.Ponge, J.C.Rosso, L.Carbonell. *J. Therm. Anal.*, **15**, 101 (1979)
84. Ch.Zhang, Y.Wu, Y.Zhang, Y.Bai, J.Gu, Y.Sun. *J. Membr. Sci.*, **508**, 136 (2016)
85. Ch.Sungkapreecha, N.Iqbal, A.M.Gohn, W.W.Focke, R.Androsch. *Polymer*, **126**, 116 (2017)
86. Y.S.Nam, T.G.Park. *J. Biomed. Mater. Res.*, **47**, 8 (1999)
87. P.van de Witte, A.Boorsma, H.Esselbrugge, P.J.Dijkstra, J.W.A.van den Berg, J.Feijen. *Macromolecules*, **29**, 212 (1996)
88. P.Shaaf, B.Lotz, J.C.Wittmann. *Polymer*, **28**, 193 (1987)
89. S.Nakano. *J. Polym. Sci.*, **12**, 1499 (1974)
90. L.A.Kleintjens, R.Konigsveld. *Macromolecules*, **13**, 303 (1980)
91. M.J.Park, S.C.Noh, C.K.Kim. *Ind. Eng. Chem. Res.*, **52**, 10690 (2013)
92. M.Y.Jeon, C.K.Kim. *J. Membr. Sci.*, **300**, 172 (2007)
93. H.Matsuyama, H.Okafuji, T.Maki, M.Teramoto, N.Kubota. *J. Membr. Sci.*, **223**, 119 (2003)
94. Zh.Wang, W.Yu, Ch.Zhou. *Polymer*, **56**, 535 (2015)
95. H.Zhang, J.Zhou, X.L.Zhang, H.T.Wang, W.Zhong, Q.G.Du. *Eur. Polym. J.*, **44**, 1095 (2008)
96. N.Tang, X.Hua, Z.Li, L.Zhang, J.Wang, J.Xiang, P.Cheng, X.Wang. *Chin. J. Chem. Eng.*, **27**, 1058 (2019)
97. H.Ding, Y.Tian, L.Wang, B.Liu. *J. Appl. Polym. Sci.*, **105**, 3355 (2007)
98. B.Zhou, Y.Tang, Q.Li, Y.Lin, Y.Miao, Y.Xiong, X.Wan. *J. Appl. Polym. Sci.*, **132**, 35 (2015)
99. D.R.Lloyd, S.S.Kim, K.E.Kinzer. *J. Membr. Sci.*, **64**, 1 (1991)
100. Zh.Yang, P.Li, L.Xie, Zh.Wang, S.Ch.Wang. *Desalination*, **192**, 168 (2006)
101. Y.K.Lin, G.Chen, J.Yang, X.L.Wang. *Desalination*, **236**, 8 (2009)
102. J.J.Kim, J.R.Hwang, U.Y.Kim, S.S.Kim. *J. Membr. Sci.*, **108**, 25 (1995)
103. I.S.Cho, J.H.Kim, S.S.Kim. *Korea Polym. J.*, **5** , 191 (1997)
104. B.Luo, S.Li, J.Zhang, X.Wang. *Desalination*, **233**, 19 (2008)
105. G.Chen, Y.Lin, X.Wang. *J. Appl. Polym. Sci.*, **105**, 2000 (2007)
106. W.Yave, R.Quijada, D.Serafini, D.R.Lloyd. *J. Membr. Sci.*, **263**, 154 (2005)
107. Y.J.Wang, Zh.P.Zhao, Zh.Y.Xi, S.Y.Yan. *J. Membr. Sci.*, **548**, 332 (2018)
108. H.K.Lee, S.C.Kim. *J. Appl. Polym. Sci.*, **67**, 159 (1998)
109. M.E.Vanegas, R.Quijada, D.Serafini. *Polymer*, **50**, 2081 (2009)
110. A.Prasad, H.Marand, L.Mandelkern. *J. Polym. Sci., Part B*, **82**, 1819 (1993)
111. M.Shang, H.Matsuyama, M.Teramoto, D.R.Lloyd, N.Kubota. *Polymer*, **44**, 7441 (2003)
112. J.A.de Lima, M.I.Felisberti. *J. Membr. Sci.*, **344**, 237 (2009)
113. B.J.Cha, K.Char, J.J.Kim, S.S.Kim, C.K.Kim. *J. Membr. Sci.*, **108**, 219 (1995)
114. I.J.Roh, S.Ramaswamy, W.B.Krantz, A.R.Greenberg. *J.Membr. Sci.*, **352**, 211 (2010)
115. S.Simone, A.Figoli, S.Santoro, F,Galiano, S.M.Alfadul, O.A.Al-Harbi, E.Drioli. *Sep. Pur. Technol.*, **90**, 147 (2012)
116. S.Ramaswamy, A.R.Greenberg, W.B.Krantz. *J. Membr. Sci.*, **210**, 175 (2002)
117. H.Karkhanechi, S.Rajabzadeh, E.Nicolo, H.Usuda, A.Shaikh, H.Matsuyama. *Polymer*, **97**, 515 (2016)
118. K.Xu, Y.Cai, N.T.Hassankiadeh, Y.Cheng, X.Li, X.Wang, Z.Wang, E.Drioli, Z.Cui. *Desalination*, **456**, 13 (2019)
119. K.Nakatsuka, Y.Ohmukai, T.Maruyama, H.Matsuyama. *Desal. Water Treat.*, **17** , 275 (2010)
120. H.Q.Liang, L.S.Wan, Zh.K.Xu. *Chin. J. Polym. Sci.*, **34**, 1423 (2016)
121. S.Rajabzadeh, T.Maruyama, T.Sotani, H.Matsuyama. *Sep. Pur. Technol.*, **63**, 415 (2008)
122. Y.Tang, Y.Lin, W.Ma, Y.Tian, J.Yang, X.Wang. *J. Appl. Polym. Sci.*, **118**, 3518 (2010)
123. M.Gu, J.Zhang, X.Wang, H.Tao, L.Ge. *Desalination*, **192**, 160 (2006)
124. Y.Lin, Y.Tang, H.Ma, J.Yang, Y.Tian, W.Ma, X.Wang. *J. Appl. Polym. Sci.*, **114**, 1523 (2009)
125. Zh.Song, M.Xing, J.Zhang, B.Li, Sh.Wang. *Sep. Pur. Technol.*, **90**, 221 (2012)
126. G.L.Ji, Ch.H.Du, B.K.Zhu, Y.Y.Xu. *J. Appl. Polym. Sci.*, **105**, 1496 (2007)
127. X.Li, G.Xu, X.Lu, Ch.Xiao. *J. Appl. Polym. Sci.*, **107**, 3630 (2007)
128. Zh.Cui, Y.Cheng, K.Xu, J.Yue, Y.Zhou, X.Li, Q.Wang, Sh.-P.Sun, Y.Wang, X.Wang, Zh.Wang. *Polymer*, **141**, 46 (2018)
129. H.Y.Ding, Q.Zhang, F.M.Wang, Y.Tian, L.H.Wang, Y.Q.Shi, B.Q.Liu. *J. Appl. Polym. Sci.*, **105**, 3280 (2007)
130. M.R.Caplan, Ch.Y.Chiang, D.R.Lloyd, L.Y.Yen. *J. Membr. Sci.*, **130**, 219 (1997)
131. A.E.Chalykh, V.K.Gerasimov, Yu.M.Mikhailov. *Diagrammy Fazovogo Sostoyaniya Polimernykh Sistem*. (Diagrams of Phase State of Polymer Systems). (Moscow: Yanus-K, 1998)
132. H.Q.Liang, Q.Y.Wu, L.S.Wan, X.J.Huang, Zh.K.Xu. *J. Membr. Sci.*, **446**, 482 (2013)
133. I.B.Rabinovich, A.N.Mochalov, L.Y.Tsvetkova, T.B.Khlyustova, Y.M.Moiseyeva, V.A.Maslova. *Acta Polym.*, **34**, 482 (1983)
134. X.He, J.Herz, J.-M.Guenet. *Macromolecules*, **22**, 1390 (1989)
135. X.He, J.Herz, J.-M.Guenet. *Macromolecules*, **20**, 2003 (1987)
136. A.B.Shipovskaya, S.Yu. Shchegolev. *Fazovyi Analiz i Opticheskaya Aktivnost' Sistem Efir Tsellyulozy – Mezofazogennyi Rastvoritel'*. (Phase Analysis and Optical Activity of Cellulose Ester – Mesophasogenic Solvent Systems). (Saratov: Saratov University, 2014)
137. B.Hagstrom. *J. Mater. Sci.*, **20**, 3906 (1985)

138. E.Calahorra, G.M. Guzman, F.Zamora. *J. Polym. Sci., Polym. Lett. Ed.*, **20**, 181 (1982)
139. P.Smith, A.J.Pennings. *J. Mater. Sci.*, **11**, 1450 (1976)
140. J.Yoon, A.J.Lesser, T.J.McCarthy. *Macromolecules*, **42**, 8827 (2009)
141. P.Smith, A.J.Pennings. *J. Polym. Sci., Polym. Phys. Ed.*, **15**, 523 (1977)
142. K.S.McGuire, D.R.Lloyd, G.B.A.Lim. *J. Membr. Sci.*, **79**, 27 (1993)
143. A.A.Alwatarri, D.R.Lloyd. *J. Membr. Sci.*, **64**, 55 (1991)
144. M.C.Yang, J.S.Peng. *J. Membr. Sci.*, **187**, 13 (2001)
145. S.R.Vippagunta, Z.Wang, S.Hornung, S.L.Krill. *J. Pharm. Sci.*, **96**, 294 (2007)
146. A.Vallee, S.Besner, J.Prudhomme. *Electrochim. Acta*, **37**, 1579 (1992)
147. S.Lascaud, M.Perrier, A.Vallee, S.Besner, J.Prudhomme. *Macromolecules*, **27**, 7469 (1994)
148. Y.L.Lee, B.Crist. *J. Appl. Phys.*, **60**, 2683 (1986)
149. G.Fu, T.Kyu. *Polymer*, **116**, 350 (2017)
150. G.Fu, S.Buddhiranon, N.Kim, A.Seko, K.Adachi, Y.Tsukahara, T.Kyu. *Polymer*, **159**, 64 (2018)
151. X.Zhu, Y.Xiao, P.He, D.Yan, Y.Fang. *Polym. Int.*, **52**, 813 (2003)
152. C.C.Grute. *J. Polym. Sci., Polym. Phys. Ed.*, **17**, 1295 (1979)
153. C.Muller, T.A.M.Ferenczi, M.Campoy-Quiles, J.M.Frost, D.D.C.Bradley, P.Smith, N.Stingelin-Stutzmann, J.Nelson. *Adv. Mater.*, **20**, 3510 (2008)
154. B.Hajduk, H.Bednarski, B.Jarzabek, H.Janeczek, P.Nitschke. *Beilstein J. Nanotechnol.*, **9**, 1108 (2018)
155. J.C.Wittmann, R.St.J.Manley. *J. Polym. Sci.*, **15**, 1089 (1977)
156. A.A.Tager. *Polym. Sci USSR*, **32**, 1939 (1990)
157. D.Dasgupta, S.Manna, S.Malik, C.Rochas, J.-M.Guenet, A.L.Nandi. *Macromolecules*, **38**, 5602 (2005)
158. D.Dasgupta, S.Manna, S.Malik, C.Rochas, J.-M.Guenet, A.K.Nandi. *Macromol. Symp.*, **222**, 175 (2005)
159. A.Sh.Cherdabayev, D.Ya.Tsvankin. *Polym. Sci. USSR*, **19**, 1426 (1977)
160. J.D.Hoffman, J.J.Weeks. *J. Res. Nat. Bureau Stand. A*, **66**, 13 (1962)
161. H.W.Starkweather. *J. Polym. Sci., Polym. Phys. Ed.*, **23**, 1177 (1985)
162. Ch.Daniel, M.D.Deluca, J.-M.Guenet. *Polymer*, **37**, 1273 (1996)
163. J.K.Yeganeh, F.Goharpey, R.Foudazi. *Macromolecules*, **43**, 8670 (2010)
164. W.R.Burghardt. *Macromolecules*, **22**, 2482 (1989)
165. M.Frankosky, J.G.Aston. *J. Phys. Chem.*, **69**, 3126 (1965)
166. H.Matsuda, R.Kashiwagi, M.Okabe. *Polymer*, **20**, 189 (1988)
167. C.Daniel, C.Dammer, J.-M.Guenet. *Polymer*, **35**, 4243 (1994)
168. L.N.Mizerovskii, K.V.Pochivalov, V.V.Afanas'eva. *Polym. Sci., Ser. A*, **52**, 973 (2010)
169. G.Rehage, D.Muller, O.Ernst. *Macromol. Chem.*, **88**, 232 (1965)
170. R.Konigsveld, A.J.Staverman. *J. Polym. Sci., Part A-2*, **6**, 305 (1968)
171. A.R.Schultz, P.J.Flory. *J. Am. Chem. Soc.*, **74**, 4760 (1952)
172. C.E.Rogers, V.Stannet, M.Szwarc. *J. Phys. Chem.*, **63**, 1406 (1959)
173. A.S.Michaels, R.W.Hausslein. *J. Polym. Sci., Polym. Phys. Ed.*, **3**, 61 (1965)
174. S.J.Doong, W.S.W.Ho. *Ind. Eng. Chem. Res.*, **30**, 1351 (1991)
175. E.F.Castro, E.E.Gonzo, J.C.Gottifredi. *J. Membr. Sci.*, **113**, 57 (1996)
176. L.V.Serna, J.L.Becker, J.R.Galdamez, R.P.Danner, J.L.Duda. *J. Appl. Polym. Sci.*, **107**, 138 (2008)
177. D.R.Sturm, K.J.Caputo, S.Liu, R.P.Danner. *Fluid Phase Equil.*, **470**, 68 (2018)
178. B.J.Savatsky, J.A.Moebus, B.R.Greenhalgh. *Macromol. React. Eng.*, 1900003 (2019)
179. T.Alfrey, H.J.Mark. *J. Phys. Chem.*, **46**, 112 (1942)
180. K.V.Pochivalov, T.N.Lebedeva, A.N.Il'yasova, A.V.Basko, Y.V.Kudryavtsev. *Fluid Phase Equilib.*, **471**, 1 (2018)
181. K.V.Pochivalov, A.N.Vyalova, R.Y.Golovanov, L.N.Mizerovskii. *Russ. J. Appl. Chem.*, **85**, 153 (2012)
182. A.N.Il'yasova, T.N.Lebedeva, A.N.Shilov, K.V.Pochivalov. *Polym. Sci., Ser. A*, **59**, 839 (2017)
183. A.N.Il'yasova, Y.V.Kudryavtsev, T.N.Lebedeva, I.V.Levashova, Y.A.Flyagina, K.V.Pochivalov. *Russ. J. Phys. Chem., A*, **91**, 425 (2017)
184. A.N.Ilyasova, G.A.Shandryuk, Y.V.Kudryavtsev, T.N.Lebedeva, M.Lutovac, K.V.Pochivalov. *Polym. Sci., Ser. A*, **58**, 1017 (2016)
185. K.V.Pochivalov, A.V.Basko, A.N.Shilov, T.N.Lebedeva, A.N.Ilyasova, G.A.Shandryuk, Y.V.Kudryavtsev. *Thermochim. Acta*, **669**, 45 (2018)
186. L.N.Mizerovskii, T.N.Lebedeva, K.V.Pochivalov. *Polym. Sci., Ser. A*, **57**, 257 (2015)
187. L.N.Mizerovskii, K.V.Pochivalov, A.N.Il'yasova. *Polym. Sci., Ser. A*, **55** , 295 (2013)
188. K.V.Pochivalov, T.N.Lebedeva, A.N.Ilyasova, A.V.Basko, Y.V.Kudryavtsev. *J. Mol. Liq.*, **283**, 366 (2019)
189. L.N.Mizerovskii, K.V.Pochivalov, T.N.Lebedeva, R.Yu.Golovanov, L.A.Antina. *Polym. Sci., Ser. A*, **57**, 389 (2015)
190. L.N.Mizerovskii, K.V .Pochivalov, Y.V.Kudryavtsev, T.N.Lebedeva, R.Yu.Golovanov, L.A.Antina. *J. Macromol. Sci., Part B: Polym. Phys.*, **54**, 1001 (2015)
191. K.V.Pochivalov, Y.V .Kudryavtsev, A.V.Basko, T.N.Lebedeva, R.Y.Golovanov. *J. Macromol. Sci., Part B: Phys.*, **54**, 1427 (2015)
192. L.N.Mizerovskii, K.V.Pochivalov, Y.V.Kudryavtsev, T.N.Lebedeva, R.Y.Golovanov, L.A.Antina. *Polym. Sci., Ser. A*, **57**, 399 (2015)
193. L.A.Antina, Y.V.Kudryavtsev, T.N.Lebedeva, K.V.Pochivalov, L.N.Mizerovskii. *Fibre Chem.*, **47**, 446 (2016)
194. K.V.Pochivalov, A.V.Basko, Y.I.Denisova, G.A.Shandryuk, A.A.Ezhov, V.V.Artemov, Y.V.Kudryavtsev. *J. Therm. Anal. Calor.*, **138**, 2481 (2019)
195. K.V.Pochivalov, Y.V.Kudryavtsev, T.N.Lebedeva, L.A.Antina, A.N.Il'yasova, A.V.Basko, A.E.Zavadskii. *J. Therm. Anal. Calor.*, **131**, 2225 (2018)
196. K.V.Pochivalov, A.V.Basko, T.N.Lebedeva, L.A.Antina, R.Yu.Golovanov, V.V.Artemov, A. A.Ezhov, Ya.V.Kudryavtsev. *Thermochim. Acta*, **659**, 113 (2018)
197. A.F.M.Barton. *Handbook of Solubility Parameters and Other Cohesion Parameters*. (Boca Raton, FL: CRC Press, 1991)
198. N.B.Vargaftik. *Spravochnik po Teplofizicheskim Svoistvam Gazov i Zhidkostei* (Handbook of Thermophysical Properties of Gases and Liquids). (Moscow: Nauka, 1972)
199. D.R.Lide. *CRC Handbook of Chemistry and Physics: a Ready Reference of Chemical and Physical Data*. (Boca Raton, FL: CRC Press, 2004)
200. A.A.Askadskii, V.I.Kondrashchenko. *Komp'yuternoe Materialovedenie Polimerov Atomno-Molekulyarnyi Uroven'*. (Computational Materials Science of Polymers. Atomic Molecular Level). (Moscow: Nauchnyi Mir, 1999). Vol. 1, 544 p.
201. B.Wunderlich. *Macromolecular Physics*. Vol. 3. (New York: Academic Press, 1980)
202. J.Arnauts, R.De Cooman, P.Vandeweerdt, R.Konigsveld. *Thermochim. Acta*, **238**, 1 (1994)
203. L.N.Mizerovskii, K.V.Pochivalov, A.N.Vyalova, O.V.Rozhkova, R.Y.Golovanov, V.P.Barannikov, A.E.Zavadskii. *Fibre Chem.*, **43**, 222 (2011)]